Inductive acceleration of UHECRs in sheared relativistic jets

Maxim Lyutikov

Department of Physics, Purdue University,

525 Northwestern Avenue West Lafayette, IN 47907-2036 ∗

Rachid Ouyed

Department of Physics and Astronomy,

University of Calgary, 2500 University Drive NW,

Calgary, Alberta, T2N 1N4 Canada

Abstract

Relativistic outflows carrying large scale magnetic fields have large inductive potential and may accelerate protons to ultra high energies. We discuss a novel scheme of Ultra-High Energy Cosmic Ray (UHECR) acceleration due to drifts in magnetized, cylindrically collimated, sheared jets of powerful active galaxies (with jet luminosity $\geq 10^{46}$ erg s^{-1}). We point out that a positively charged particle carried by such a plasma is in an unstable equilibrium if $\mathbf{B} \cdot \nabla \times \mathbf{v} < 0$, so that kinetic drift along the velocity shear would lead to fast, *regular* energy gain. This can be achieved in an axially inhomogeneous jet through gradient drift induced by propagation of inertial Alfvén waves along the jet. We show that if a seed of pre-accelerated particles with energy below the ankle $\leq 10^{18}$ eV is present, these particles can be boosted to energies above 10^{19} eV. A key feature of the mechanism is that the highest rigidity (ratio of energy to charge) particles are accelerated most efficiently implying the dominance of light nuclei for energies above the ankle in our model: from a mixed population of pre-accelerated particle the drift mechanism picks up and boosts protons preferably. In addition, after a particle traversed large fraction of the available potential, its Larmor radius becomes of the order of the jet thickness. In this case, *the maximum possible acceleration rate of inverse relativistic gyro-frequency is achieved* and a particle finally become unconfined and leave the jet. The power-law spectrum of the resulting UHE particles flattens with time and asymptotically may become $\propto E^{-2}$. The real injection spectrum depends on the distribution of pre-accelerated particles inside a jet and, in case of contribution from many sources, on the distribution of total potential drop.

We also point out that astrophysical schemes based on DC-type acceleration (by electric field parallel to or larger than magnetic field) cannot have potentials larger than $\sim 10^{15}$ Volts and thus fell short by many orders of magnitude to produce UHECRs.

---

*Electronic address: `lyutikov@purdue.edu`

I. INTRODUCTION

Acceleration of Ultra High Energy Cosmic Rays (UHECRs), with energies reaching 3×10^{20} eV, remains one of the main challenges of modern physics and astrophysics [1–5]. UHECRs can be either accelerated by "astrophysical Zevatrons" (or bottom-up scenario) or a be a by-product of decay of massive exotic particles (top-down scenario).

The most commonly discussed astrophysical mechanism of acceleration of UHECRs is diffuse shock acceleration by relativistic shocks [6, 7] where small scale magnetic field, amplified typically to near-equipartition (see §II), are required. In addition, it is necessary that scattering rate is close to the maximum (Bohm) rate in order to overcome advection of particles downstream of a shock. It is far from clear whether such rates are achievable [8].

Commonly, it is believed that low energy cosmic rays, with energies approximately below the "ankle" at $\sim 10^{18}$ eV, are of Galactic origin (GCR), while those above the "ankle" are extragalactic. [Note, that exact location of transition between Galactic and extragalactic cosmic rays is not clear and may instead be associated with the "second knee", [9].] Since spectra below and above the "ankle" are different, different acceleration mechanisms should operate [see 10, for an alternative holistic scenario]. In this paper we propose new mechanism that operates at highest energies and thus is responsible for extragalactic cosmic rays (EGCR): particle acceleration by inductive electric fields in magnetized, relativistic sheared outflows.

Inductive electric fields and cosmic ray acceleration has been mentioned by many authors [1, 11–13], but no concrete acceleration mechanism has been proposed (with a possible exception of [14], see below). It was only pointed out that there is a large electric potential and it was *assumed* that particle somehow manage to tap it. Since inductive electric fields are orthogonal to magnetic field and particles cannot move freely along them, it is not obvious how to achieve energy gain. Another acceleration scheme is acceleration in DC electric field aligned with magnetic fields (double layers), but these, as we demonstrate in appendix A, cannot account for UHECRs.

A. Inductive electric fields

As mentioned above, inductive electric fields are not easily accessible for acceleration since particle need to move across magnetic field, a processes prohibited under ideal Magneto-Hydrodynamics (MHD) approximation. On the other hand, kinetic drifts may result in regular motion across magnetic field and along electric field leading to *regular energy gain* as compared to the stochastic, Fermi-type schemes. Since the drift velocity increases with particle energy, *the rate of energy gain will also increases with particle energy.* Thus, the highest energy particles will be accelerated most efficiently. This means that from a pre-accelerated population, the mechanism proposed here will pick up particles with highest energy and will boost them to even higher values. In addition, when a particle has crossed a considerable fraction of the total available potential, it gyro-radius becomes comparable with flow scale (§II). In this case, drift approximation brakes down. As a result, as long as the particle remains inside a jet, *the acceleration rate reaches the theoretical maximum of an inverse gyro-frequency (§V B).* Thus, the most efficient acceleration occurs right before the particle leaves the jet. One may say that in case of inductive acceleration, *becoming unbound is beneficial to acceleration*, contrary to the case of stochastic acceleration when for unbound particles acceleration ceases.

Typically, the direction of drift is along the normal to the magnetic field and to the direction of the force that induces a drift. In sheared cylindrical jet with toroidal magnetic field electric field is in radial direction, so that in order to gain energy particle should experience radial drift. It is then required that there should be a force along the axis. Such force may arise if a jet is axially inhomogeneous resulting in gradient drift due to changing magnetic pressure. Several types of inhomogeneity can occur in astrophysical jets. Numerical simulations of hydromagnetic jets show complicated axial structure with regions of compression and rarefaction [15–17]. Besides shocks, these simulations show prominent subsonic density and magnetic field variations inside jets. Subsonic variations propagate roughly with the jet flow and induce axial variations of magnetic field leading to radial drifts. An important property of the mechanism proposed here is that for a particle at rest with respect to the bulk flow energy gain (or loss) is *independent* of the direction of the drift (*e.g.* away or towards the axis; see §V). On the other hand, if an axial variation is periodic, *e.g.* a wave, changing the direction of the drift would lead to alternative energy gains and losses. If in

one wave period a high energy particle acquires a large enough energy so that its gyro-radius becomes comparable to jet scale, it will leave the jet.

B. Electric drifts and particle acceleration

To separate effects of electric drift in crossed electric and magnetic fields (which does not lead to energy gain) and particle acceleration, we should consider particle dynamics in a local plasma rest frame, where electric field vanishes at the origin. Since the velocity field is likely to be sheared (*e.g.* higher velocity near the axis of a jet), there will be non-vanishing electric field away from the origin. Value of the electric field at a position of a particle will be smaller than inductive field in the laboratory frame, approximately, by a ratio of Larmor radius to shear scale. Typically, both shear velocity and electric field would be linear function near the origin, so that *electric potential is a quadratic function of distance from the origin of the local plasma rest frame.* Depending on the sign of the coefficient in front of the quadratic term, electric potential has either a minimum or maximum near the origin. This depends on the sign of the charge and sign of the product $\mathbf{B} \cdot \nabla \times \mathbf{v}$. In §III we show that *in sheared flows with $\mathbf{B} \cdot \nabla \times \mathbf{v} < 0$ protons are near the maximum of electric potential*, so that drift motion away from the origin (*along or against* the direction of the shear), will lead to energy gain.

Our model bears some resemblance to Bell model [14] of cosmic ray acceleration at pulsar wind nebular, which relies on large (unreasonably large, in our view) magnetic field gradients near the axis of the expanding flow in order to "pull-in" pre-accelerated charges against weakly relativistic expansion of plerion. The proposed mechanisms also has both similarities and differences from the shock drift acceleration at non-parallel shocks [18]. A shock can be considered as an extreme case of field inhomogeneity (a delta-function), so that drift velocity is a delta function [19]. This can similarly produce energy gains due to displacements of particle along inductive electric field associated with shock motion. The idea that particle energy can be limited by "lateral" escape, is also reminiscent of Eichler model [20] of particle acceleration at the Earth's bow shock. The difference is that in Eichler's model the sideways motion of a CR was due to cross-field diffusion, while in our case it is a gradient drift.

Our acceleration scheme is also very different from those previously considered in sheared flows due to second-order Fermi process [3, 21–23]. In the references cited above particle

energetization occurs due elastic scattering by magnetic field inhomogeneities in the flow rest frame. Acceleration is stochastic, while acceleration time scales are typically very long, scaling as velocity shear squared, V'^2, [22], so that extremely narrow layers are required. Contrary to this, in our scheme acceleration is regular and scales as V'.

Let us also point out that any acceleration scheme based on DC-type acceleration, where there is large electric field along magnetic field or where electric field becomes larger than magnetic field, cannot accelerate particles to energies above 10^{15} eV, appendix A. This excludes, for example, magnetic reconnection [24, 25].

In this paper we start in Section 2 by briefly describing on general basis the properties of UHECR acceleration sites. The constraints on source energetics and size are discussed within the context of cylindrical AGN jets. In Section 3 and 4 we study the evolution of particles trapped in sheared flows and in the presence of Alfvén waves. The details of the acceleration mechanisms at play are described in details in Section 5. The corresponding particle spectrum is derived in Section 6 before considering the astrophysical implications in Section 7. A discussion is presented in Section 8 and a brief conclusion in Section 9.

II. AGN JETS AS POSSIBLE SITES OF UHECR ACCELERATION

A. Luminosity - Potential relation

In bottom-up acceleration schemes [4, 26] any source that accelerates a particle to a particular energy should have a total electric potential drop of the same order (it is unlikely that a particle completes many circuits with much smaller potential drops). On very basic grounds, we expect that in any astrophysical system electric field are no larger than magnetic field. [Localized gaps, regions with either parallel electric field or total electric field larger than magnetic, may exist but the typical potential drop in them is small (for purposes of UHECR acceleration) and is limited by lepto-photonic pair production, [27].] This has two consequences. First, regardless of the acceleration mechanism, the highest possible acceleration rate is inverse of the relativistic gyro-frequency, $\sim \gamma/Z\omega_B$ where $\omega_B = eB/mc$ is cyclotron frequency, Z is a charge of a particle in terms of elementary charge e, m is a mass of a particle. Secondly, we can place very general constraints on possible accelerating sites [see also 28]. If we parameterize $E = \beta_0 B$ where E is the electric field and B is the

magnetic field (β_0 is the ratio of typical electric to magnetic fields) and if an accelerating region has a size R the available potential is $\Phi \sim RE \sim \beta_0 RB$ and the energy of particle crossing that potential would be

$$\mathcal{E} = Ze\beta_0 BR \tag{1}$$

For $\beta_0 \sim 1$ this is also the condition that the particle's gyro-radius is smaller than R [29]. Thus, for $\beta_0 \sim 1$, a system will be able to accelerate particles to the maximum energy that it can confine. We would like to stress that the conditions on acceleration of UHECRs (1) are different from confinement condition $r_L < R$, where r_L is the Larmor radius. The two conditions are different by a factor β_0: for $\beta_0 \ll 1$ a system can confine particles with energies much larger than those to which it can accelerate.

Since BR is a measure of the total current in the system, Eq. (1) can be rewritten as (assuming $\beta_0 \sim 1$)

$$\Phi = \beta_0 \frac{2I}{c} \tag{2}$$

This determines the maximum electric potential and corresponding energy $\mathcal{E} = Ze\Phi$ to which a system carrying a current I can accelerate.

Unless the electric field is strictly along the magnetic field (*e.g.* in double layers, see appendix A), there is Poynting flux in the system. Since Poynting flux cannot be larger than the total luminosity of a given source, assuming a spherical expansion we find

$$L = 4\pi R^2 \frac{1+\sigma}{\sigma} \frac{EB}{4\pi} c \sim \frac{1+\sigma}{\sigma} R^2 B^2 \beta_0 c = \frac{1+\sigma}{\sigma} \frac{1}{\beta_0} \Phi^2 c \tag{3}$$

where σ is the ratio of Poynting to particle flux [30]

Thus, assuming $\beta_0 \sim 1$,

$$\Phi \leq \sqrt{\frac{\sigma}{1+\sigma}} \sqrt{\frac{4\pi L}{c}} = 4 \times 10^{20} \mathrm{V} L_{46}^{1/2}$$

$$I \leq \sqrt{\frac{\sigma}{1+\sigma}} \sqrt{\frac{Lc}{4\pi}} = 3.6 \times 10^{25} \mathrm{A} L_{46}^{1/2}$$

$$L = \frac{1+\sigma}{\sigma} I\Phi \tag{4}$$

where we introduced coefficients of the order of unity so that in the limit $\sigma \to \infty$ the system impedance is that of free space, $4\pi/c$; $L_{46} = L/10^{46}$ erg/s and for numerical estimate we assumed $\sigma = 1$. For each particular system these relations will be modified by a numerical factor which depends on geometric properties of the system. The case of cylindrically collimated AGN jets is considered in §II B.

7

Eq. (4) relates the maximum available potential to the luminosity of the source. Assuming that UHECRs are protons, we can select possible candidates for UHECRs acceleration based on their luminosity: to achieve 3×10^{20} eV we need $L \geq 10^{46}$ erg/s. We can immediately *exclude acceleration of UHECRs in low power AGNs (e.g. Cen A and M87), low power BL Lacs and starburst galaxies (e.g. M82 & NGC 253)* (in case of proton component), see also §VII. This limits the possibilities to more distant high power AGNs like higher power FR I, FR II radiogalaxies, radio-loud quasars and GRBs. [In appendix B we argue against GRB shocks as source of UHECRs.] Luminosity constraint (4) also excludes, in our view, holistic scenario, [10], where the same acceleration mechanism operates in all galaxies, including our own. Only "special" galaxies, satisfying condition (4) are able to accelerate UHECRs. Note, that in order to maximize potential at a given luminosity, it is required that $\sigma \geq 1$, but not necessarily $\gg 1$.

Another constraint that acceleration sites should satisfy is that radiative losses should not degrade particle energy. We can derive very general constraints on possible location of cosmic ray acceleration just by balancing most efficient acceleration, by $E \sim B$, and radiative losses [see also 31]. Typically, radiative losses scale as $\propto \gamma^2 u$ where γ is the Lorentz factor of a cosmic ray and u is energy density of the medium that leads to radiative losses. For synchrotron losses $u = u_B = B^2/8\pi$, for IC losses $u = u_{IC}$ is the energy density of soft photons. If we normalize total energy density to energy density of magnetic field $u = \zeta u_B$, $\zeta > 1$, and equate the maximal rate of energy gain $d\mathcal{E}/dt = ZecE \sim ZecB$ to radiative losses $d\mathcal{E}/dt \sim \frac{Z^4 e^2}{c} \omega_B^2 (\mathcal{E}/mc^2)^2$ we find

$$\mathcal{E} = mc^2 \sqrt{\frac{c}{\zeta r_c Z^3 \omega_B}} \tag{5}$$

where $r_c = e^2/mc^2$. This may be considered as a second constraint on the site of particle acceleration. Resolving eqns (1) and (5) with respect to B and R we find

$$B < \frac{m^2 c^4}{\zeta Z^3 e^3} \left(\frac{mc^2}{\mathcal{E}}\right)^2 \Gamma^3 = 2\,\Gamma^3\,\mathrm{G}\,\left(\frac{\mathcal{E}}{100 EeV}\right)^{-2} \left(\frac{1}{Z}\right)^3$$
$$R > \frac{Z^2 e^2 \zeta}{mc^2} \left(\frac{\mathcal{E}}{mc^2}\right)^3 \frac{1}{\Gamma^2} = 10^{17}\,\frac{1}{\Gamma^2}\,\mathrm{cm}\,\left(\frac{\mathcal{E}}{100 EeV}\right)^3 (Z)^2 \tag{6}$$

Where we also allowed a possibility that plasma is expanding with bulk Lorentz factor Γ, so that magnetic field in the plasma rest-frame is B/Γ and typical scale is R/Γ, and assumed $\zeta = 1$; $EeV = 10^{18}$ eV.

8

Relations (6) show that higher energy cosmic rays are better accelerated at large distances. AGN jets, which propagate to more than 100 kpc distances present an interesting possibility. Note, that as long as the jet remains relativistic, the total inductive potential is approximately conserved, so one can "wait" a long time for a particle to get accelerated without worrying about radiative loses. Thus, UHECRs can be accelerated inside the jet at distances from a fraction of a parsec (Eq. (6)) to hundreds of kpc, as long as the jet remains relativistic and sustains a large inductive potential.

B. Cylindrical AGN jets

As an illustration of the general principles discussed above let us consider force-free cylindrically collimated jets. A possible structure of such a jet is a relativistic sheared diffuse pinch

$$
\begin{aligned}
B_\phi &= \frac{r/R_c}{1 + (r/R_c)^2} B_0 \\
E_r &= \sqrt{1 - 1/\Gamma(r)^2} B_\phi \\
B_z &= \frac{1}{1 + (r/R_c)^2} B_0
\end{aligned}
\tag{7}
$$

where R_c is a radius of a current-carrying core. System remains in force-balance for arbitrary $\Gamma(r)$ [32]. Alternatively, instead of B_z particle pressure may ensure force-balance.

For illustration purposes let us choose a Lorentz factor with a profile,

$$
\Gamma(r) = \sqrt{1 + \frac{\Gamma_c^2 - 1}{1 + (r/R_c)^2}}
\tag{8}
$$

where $\Gamma_c = 1/\sqrt{1 - \beta_c^2}$ is the Lorentz factor of the fast core and we assumed that Lorentz factor changes on the scale of the core radius. Then the total potential is

$$
\Phi_{tot} = B_0 R_c \mathrm{arctanh}(\beta_c) \approx \frac{B_0 R_c}{2} \ln \frac{2}{1 - \beta_c},
\tag{9}
$$

while total the Poynting flux is

$$
L = \frac{B_0^2 R_c^2 c}{4} \left(\frac{1 + \beta_c^2}{\beta_c^2} \mathrm{arctanh}(\beta_c) - \frac{1}{\beta_c} \right) \approx \frac{B_0^2 R_c^2 c}{4} \ln \frac{2}{1 - \beta_c}
\tag{10}
$$

where the last equalities assume $\beta_c \to 1$. Thus

$$
\Phi_{tot} = \sqrt{\frac{L}{c}} \sqrt{\ln \frac{2}{1 - \beta_c}} \approx \sqrt{\frac{L}{c}} \sqrt{2 \ln 2\Gamma_c}
\tag{11}
$$

9

If a particle start on the axis with $\gamma = \gamma_c$, and drifts in a radial direction, its Lorentz factor γ changes with radius as

$$\gamma = \gamma_c + \frac{\omega_{B,0} R_c}{c} \left(\mathrm{arctanh}\beta_c - \mathrm{arctanh}\frac{\beta_c}{1 + (r/R_c\Gamma_c)^2} \right) \tag{12}$$

so that the particle gains large fraction of the potential after reaching $r \sim R_c\Gamma_c$. At this point its Larmor radius r_L would become

$$\frac{r_L}{R_c\Gamma_c} \sim \mathrm{arctanh}\beta_c \geq 1 \tag{13}$$

This illustrates an important point: after a particle has crossed a large fraction of the total available potential, its Larmor radius becomes comparable to the flow scale, so that it will decouple from the flow.

III. POTENTIAL ENERGY OF A CHARGE IN SHEARED FLOW

Our model of UHECR acceleration relies on the observation that in a transversely sheared flow one sign of charges is located at a maximum of electric potential, as we describe in this section. Consider sheared flow carrying magnetic field. At each point there is electric field $\mathbf{E} = -\mathbf{v} \times \mathbf{B}/c$, so that the electric potential is determined by

$$\Delta\Phi = \frac{1}{c}\nabla \cdot (\mathbf{v} \times \mathbf{B}) = \frac{1}{c}\left(\mathbf{B} \cdot (\nabla \times \mathbf{v}) - \mathbf{v} \cdot (\nabla \times \mathbf{B})\right) \tag{14}$$

In a local rest frame, the second term in Eq. (14) vanishes at the position of a particle and is generally sub-dominant to the first term for $v \ll c$ [84]. Then $\nabla \times \mathbf{B} = 0$ and we find [85]

$$\Delta\Phi = \frac{1}{c}\left(\mathbf{B} \cdot \nabla \times \mathbf{v}\right) \tag{15}$$

We have arrived at an important result: *depending on the sign of the quantity $(\mathbf{B} \cdot \nabla \times \mathbf{v})$ (which is a scalar) charges of one sign are near potential minimum, while those with the opposite sign are near potential maximum.* Since electric field is perpendicular both to velocity and magnetic field, locally, the electric potential is a function of only one coordinate along this direction. For $(\mathbf{B} \cdot \nabla \times \mathbf{v}) < 0$ (we will call this case negative shear) ions are near potential maximum.

The procedure outlined above to calculate electric potential is beyond the limits of applicability of *non-relativistic* MHD, which assumes quasi-neutrality and thus neglects the

10

dynamical effects associated with the potential (15). Thus, even in the low frequency regime with non-relativistic velocities, a conventional realm of MHD theory, one should use at least two fluid approach and also must retain both charge density as well as displacement current in Maxwell equations.

We can arrive at a more general result using a relativistic MHD formulation. An invariant charge density is given by

$$\rho = j^\mu u_\mu = \frac{1}{4\pi} F^{\mu\nu}_{,\nu} u_\mu \tag{16}$$

where j^μ is four-current, u_μ is fluid four-velocity and $F^{\mu\nu}$ is the electromagnetic tensor and Greek indexes run $0, 1, 2, 3$ and we set speed of light to unity here. In the framework of relativistic MHD, when stress-energy tensor is diagonalizable, the electromagnetic tensor can be written as $F^{\mu\nu} = \epsilon^{\mu\nu\alpha\beta} B_\alpha u_\beta$, where B_α is a four-vector of magnetic field and $\epsilon^{\mu\nu\alpha\beta}$ is a unit antisymmetric tensor. Charge density becomes

$$\rho = \frac{1}{4\pi} \epsilon^{\mu\nu\alpha\beta} u_\mu \left(B_{\alpha,\beta} u_\beta + B_\alpha u_{\beta,\nu} \right) \tag{17}$$

If the magnetic field is stationary and homogeneous, $B_{\alpha,\beta} = 0$, then we arrive at

$$\rho = \frac{1}{4\pi} F^{\mu\nu} u_{\mu,\nu} \tag{18}$$

which generalizes Eq. (15) to an invariant form.

Under ideal fluid approximation particles cannot move across magnetic field lines, so that they cannot "sample" the electric potential (15). On the other hand, kinetic effects, like drift motions, may lead to regular radial displacement along the shear and thus along electric field. In this case one sign of charge will be gaining energy, while another sign will be losing energy. This is independent on whether the drift is along the shear or counter to the shear direction and thus is independent on the sign of the magnetic field gradient that induces the shear.

For low energy particles, with small but finite Larmor radii, variations of potential energy need to be taken into account for a correct description of the plasma distribution function in magnetized flows with transverse shear [34–36]. [Since the distribution function should depend on constants of motion, in presence of a velocity shear these constants are different from the case of no shear.] Kinetic motion allows particle to probe regions with different potential and lead to redistribution of positive and negative changes in an effort to screen the shear-induced electric field. These effects are absent if background plasma is cold. On

11

the other hand, for a small population of high energy particles with large Larmor radii, electrostatic potential (15) may become important.

IV.   ACCELERATION MECHANISM IN A NUTSHELL

Our key point is that an electrostatic cross-field potential (15) may be used for particle acceleration. In this Section we briefly outline the principal astrophysical and plasma physical issues related to this acceleration mechanism. In appendix C and §V we elaborate in more details the qualitative statements made in this Section.

There is a consensus that relativistic outflows, and AGN jets in particular, are accelerated to relativistic speeds and collimated by large scale magnetic fields threading accretion disk and central black hole. This is based mostly on theoretical and numerical models of jet launching from black hole– accretion disk systems [37–40]. In addition, polarization properties of parsec scale AGNs jets [32] and, possibly, GRBs [41] are also consistent with the presence of large scale magnetic field. Energetically, magnetic fields may carry a large fraction of jet luminosity [42, 43], so that the parameter σ introduced above is not too small, $\sigma \geq 1$.

As the jet expands, the ratio of toroidal to poloidal magnetic field increases approximately linearly with cylindrical radius of a jet, so that at largest scales magnetic field is dominated by a toroidal component B_ϕ. In addition, toroidal magnetic field may provide jet collimation, so that asymptotically AGN jets may also be fully collimated to a cylindrical shape [44]. One also expects that jets are sheared, so that the central spine of the jet is moving with larger velocity than its periphery [45–47], so that $v_z = v_z(r)$ (r is the radial coordinate in cylindrical geometry) is decreasing outward. In this case, $(\mathbf{B} \cdot \nabla \times \mathbf{v}) = -B_\phi \partial_r v_z$. If, in addition, the jet is inhomogeneous along the axis, $B_\phi = B_\phi(z)$, there will be a gradient drift along r, which in case of negative shear would lead to proton acceleration. In another type of jets, with positive shear $(\mathbf{B} \cdot \nabla \times \mathbf{v}) > 0$, electrons are accelerated while protons lose their gyrational energy eventually coming to a rest with respect to the bulk flow.

An important requirement on the proposed acceleration scheme is that the flow be nearly cylindrically collimated. This stems from the fact that as long as a particle has not crossed the total available potential, its drift velocity is non-relativistic, so that in conically expanding relativistic flows energy gain cannot compete with adiabatic losses.

Next we discuss the salient properties of kinetic particle drift motion and energy gain in sheared flows. Consider a plane-parallel sheared flow in which the magnetic field is perpendicular to the velocity. For definiteness, let magnetic field be directed along x axis, $B_x = B_0$ and velocity along z axis, $V = V_z(y)$ (see Fig. 2). Let us transform to a frame moving with the fluid at some particular values of $y = y_0$, e.g. at $y_0 = 0$. Expanding velocity near $y = 0$, $V_z = \beta_0 cy/L_V$, where β_0 is characteristic velocity in terms of speed of light and L_V is a characteristic scale. Thus, there is electric field $\mathbf{E} = -V_z B_x/c\vec{e}_y = -(V_0/c)B_0 y/L_V \vec{e}_y = -\beta_0 B_0 y/L_V \vec{e}_y$ and electric potential

$$\Phi = \beta_0 B_0 \frac{y^2}{2L_V} \tag{19}$$

Next, assume that there is a long wavelength inertial Alfvén wave propagating along the z-direction with a phase speed V_A. For $V_A \ll c$, the magnetic perturbation δB in the wave is much larger than electric perturbations δE by a factor c/V_A, so that the wave is nearly magneto-static (in other words $\omega \ll k_z c$). A test particle will experience a drift in the x-direction with magnitude

$$u_d \sim \frac{\delta B}{B_0} \frac{\gamma c^2 k_z}{Z\omega_{B,0}} \sim \frac{\gamma c^2 k_z}{Z\omega_{B,0}} \tag{20}$$

where we assumed strong perturbation $\delta B_0 \sim B$ and $\omega_{B,0} = eB_0/mc$. As a particle drifts along electric field in the x-direction its Lorentz factor evolves according to

$$\partial_t \gamma = \frac{ZeE_y u_d}{mc^2} = \beta_0 \frac{Z\omega_{B,0}u_d^2 t}{cL_V} \sim \beta_0 \frac{\gamma^2 c^3 k_z^2 t}{Z\omega_{B,0}L_V} \tag{21}$$

Thus, energy gain or loss of a test particle depends on direction of magnetic field, sign of charge (through ω_B) and direction of velocity vorticity (through sign of L_V): in other words it depends on sign of shear. On the other hand, it is *independent* of the direction of the drift.

Since drift velocity increases with particle energy, the rate of energy gain also increases with energy, see Eq. (21). This leads to one of the most unusual properties of the proposed acceleration mechanisms: *highest energy (or highest rigidity) particles are accelerated most efficiently.* In addition, at the last stages of acceleration, when particle Larmor radius becomes of the order of jet scale, particle motion in positive shear flow becomes unstable even without gradient drift while *acceleration rate does reach absolute theoretical maximum of inverses relativistic gyro-frequency* (§V B).

In addition, since acceleration rate is *inversely* proportional to charge, at a given energy small charge (higher rigidity) particles are accelerated most efficiently. Thus, from a population of pre-accelerated particles with mixed composition, drift mechanism will pick up particles with smallest charge: protons. This explains why above the ankle protons start to dominate over heavy nuclei.

Above is the upshot of the proposed acceleration mechanism. Next we elaborate its details. In appendix C we consider properties of electromagnetic waves in transversely sheared cold plasma; this is required to in order to set up correctly the background electromagnetic fields for the drift motion of a particle. In §V we consider drift motion of test particle in an electromagnetic fields of a low frequency inertial Alfvén wave propagating in a sheared flow in case of weak shear, when particle gyro-radius is much smaller than shear scale. This is done analytically for weak waves and numerically for strong waves. In §V B we consider particle motion for strong shear, when shear scale is comparable to gyro-scale, so that drift approximation is inapplicable. In this case a new type of acceleration mechanism turns on, which does not require presence of velocity-aligned magnetic field gradients and which leads to theoretically maximal acceleration rate on inverse of relativistic gyro-frequency.

V.   DETAILS OF THE ACCELERATION MECHANISM

A.   Stage 1: Kinetic drift

1.   Kinetic drift in linear Alfvén waves

In this Section we first consider kinetic motion of a particle in a combined electromagnetic fields of sheared flow and a low frequency inertial Alfvén wave propagating along velocity. For simplicity we concentrate on planar problem and assume a linear velocity profile. Using results of appendix C, electromagnetic fields of the inertial Alfvén are then given by

$$\delta E_y = aB_0 \sin\left(k_z(z - (V_A - V_z)t)\right)$$
$$\delta B_x = -\frac{aB_0 c}{V_A - V_z} \sin\left(k_z(z - (V_A - V_z)t)\right) \tag{22}$$

where a is a non-linearity parameter of the wave, defined here as a ratio of electric field amplitude to background magnetic field. Assuming linear shear, $V_z = \eta y$, Eq. (22) gives

$$E_y = B_0 \left(-\frac{\eta y}{c} + a \sin k_z (z - (V_A - \eta y)t) \right)$$
$$B_x = B_0 \left(1 - \frac{ac}{V_A - y\eta} \sin k_z (z - (V_A - \eta y)t) \right) \tag{23}$$

where $\eta = V'$ and we assumed that a test particle is located near the zero wave phase.

The equations of motion of a test particle are

$$\partial_t (\gamma \partial_t \mathbf{r}) = \frac{Ze}{mc^2} \left(\mathbf{E} + \frac{\partial_t \mathbf{r}}{\gamma c} \times \mathbf{B} \right) \tag{24}$$

Next, we separate particle motion into slow guiding center motion $\mathbf{R}(t)$ and fast rotation $\xi(t)$

$$\mathbf{r} = \mathbf{R}_0(t) + \xi(t) \tag{25}$$

with $|\xi|$ of the order of Larmor radius $\sim r_L$. Assuming long wavelength perturbations $k_z \to 0$, weak perturbing wave $a \to 0$, and expanding in small gyro radii $r_L = \sqrt{\gamma_0^2 - 1}/\omega_B$ (we neglect motion along magnetic field, $p_x = 0$), we find equations of motion of the gyrations center,

$$\partial_t^2 Y_0 = \frac{Z\omega_B}{\gamma_0} \partial_t Z_0 + \frac{Z\omega_B}{\gamma_0} \frac{\eta Y_0}{2} - k_z t (Z\omega_B V_A^2 / \gamma_0 - \eta) \frac{\delta E}{2B_0 V_A}$$
$$\partial_t^2 Z_0 = -\left(\frac{Z\omega_B}{\gamma_0} - \eta \right) \partial_t Y_0 + k_z \frac{\delta E}{2B_0 V_A} \tag{26}$$

where capital letters denote coordinates of $\mathbf{R}_0$. Equations (26) can be integrated to give a drift in the y-direction with velocity

$$\frac{U_d}{c} = a \frac{c}{V_A} \frac{k_z c \gamma_0}{2Z\omega_B} \frac{1 - (V_A/c)^2 + \eta \gamma_0/(Z\omega_B)}{1 - \eta \gamma_0/(Z\omega_B)} \approx a \frac{c(1 - (V_A/c)^2)}{V_A} \frac{k_z c \gamma_0}{2Z\omega_B} \tag{27}$$

where we have reinstated the speed of light explicitly and the last approximation assumes small $\eta \to 0$. In addition, there is insignificant motion along z which results in a z displacement of the order of $k_z \delta z \sim a(c/V_A) \leq 1$.

The origin of terms in Eq. (27) can be easily understood: $a(c/V_A)$ is a relative amplitude of magnetic field perturbations due to presence of the wave, $k_z c \gamma_0 / 2\omega_B$ is a ratio of particle Larmor radius to inhomogeneity scale and the last terms represent relativistic and shear corrections. Note, that as plasma becomes strongly magnetized, $V_A \to c$, value of the drift

15

velocity decreases. This can be understood by noting that for subluminal waves there is always a frame where electric field is zero and magnetic field is constant [48]. What is important for drift motion is the value of the magnetic field in that frame. For shear Alfvén waves this frame is moving with the velocity V_A. For $V_A \to c$, the value of magnetic field in this frame decreases which leads to smaller transverse drift velocity.

For order-of-magnitude estimates, we can assume $V_A \sim c$. [Note that for $V_A \ll c$, for a given potential total energy flux increases by $(V_A/c)^2$, while for $V_A \to c$ drift velocity becomes small, so that the mechanism operates best at $V_A \leq c$.] Then

$$\frac{U_d}{c} \sim a\frac{k_z c \gamma_0}{2Z\omega_B} \tag{28}$$

The energy of a particle changes both due to shear-induced electric field as well as the electric field of the perturbing wave. We are interested in the former contribution; the latter process – gradient drift along the electric field of the wave gives a well known surfing mechanism of particle acceleration [49]. Energy gain in such a process is limited by electric field of the wave and spatial dimension of the wave. Thus, if wave amplitude is of the order of unity, $\delta B/B \sim 1$ wave surfing will lead to similar energy gains as drift in a sheared flow. In astrophysical applications we expect $\delta B/B \leq 1$, so that shear-induced potential is typically larger than the electric potential associated with perturbing wave; see also §V A 2 for more detailed discussion of effects of surfing.

Assuming that a particle keeps coherence with the wave (see §V A 2), its energy in a shear-induced electric field evolves according to

$$\partial_t \gamma = \frac{a^2}{4}\frac{\gamma^2 c^3 t}{ZL_B^2 L_V \omega_B} \tag{29}$$

where we introduced inhomogeneity scale of magnetic field $L_B = 1/k_z$ and shear scale $L_V \sim c/V' = c/\eta$. Note that variations of energy are independent of the sign of magnetic field gradient L_B, but depend on particle charge, magnetic field and electric field gradient.

Eq. (29) implies very fast energy growth:

$$\gamma = \frac{\gamma_0}{1 - (\gamma_0/Z)(t/\tau_0)^2} \tag{30}$$

where

$$\tau_0 = \frac{2\sqrt{2}}{a}\frac{L_B}{c}\sqrt{\frac{L_V}{c/\omega_B}} \tag{31}$$

16

Note that *the acceleration time scale is inversely proportional to the square root of initial particle energy:*

$$\tau_{acc} = \frac{\tau_0 \sqrt{Z}}{\sqrt{\gamma_0}} \tag{32}$$

Thus, more energetic particles with smaller charge are accelerated on shorter time scales.

Initially the energy grows quadratically with time. At later times, the Larmor radius of a particle starts to increase in response to increasing energy. This leads to faster drift and faster rate of energy gain, which formally becomes super-exponential (finite time singularity). Of course, in order to get infinite energy a particle should move infinitely far, so that in reality maximum energy gain will be limited by the size of the system and it's total available potential. In addition, before the finite time singularity is reached, drift approximation will break down. This will occur when the particle Larmor radius becomes of the order of inhomogeneity scales L_B, L_E. This happens only a short time before finite time singularity, at times

$$t = \tau_{acc} \sqrt{1 - \frac{\gamma_0 c/\omega_B}{Z(L_B, L_V)}} \sim \tau_{acc} \tag{33}$$

2. Nonlinear waves: effects of wave surfing on energy gain

We have shown that if a particle can keep in phase with the wave in a combined electromagnetic fields of sheared flow and inertial Alfvén wave, its energy increases at super-exponential rate. In case of a linear wave this assumption is not completely satisfied: the acceleration time scale (32) is longer than the wave period by a factor $\sqrt{L_V/r_L}$. This difficulty may be overcome if perturbing wave is non-linear, with finite relative amplitude $a = \delta E/B_0$. In this case the particle will also experience a drift in crossed $\delta \mathbf{E}$ and $\mathbf{B}_0$ fields. If a particle is located at such phase of the wave so that this drift velocity is along the direction of propagation, it may remain in resonance for a long time. For substantially strong waves the longitudinal drift velocity (along the direction of wave propagation) $u_z \sim \delta E/B_0$ may become of the order of the phase velocity of the waves. Such particles are effectively trapped by the wave. In surfing acceleration schemes this leads to particle energy gain as it drifts along the electric field of the wave. In our case trapping leads to nearly constant velocity drift along the shear-induced electric field.

To test this possibility we consider numerically particles motion in a sheared flow with finite amplitude inertial Alfvén wave. As a test case, we consider planar problem, similar

to the one described in Fig. 2. For background velocity profile we chose $v_z = V_A \tanh(y/y_s)$, where y_s is a parameter determining the strength of the shear. On top of the shear we impose an inertial Alfvén wave, with fluctuating fields given in the WKB approximation (appendix C) by Eqns (22). We then seed the wave with test particle at random phases in the wave and follow their trajectory. Results of simulations are presented in Fig. 5 where we plot the maximal energy gained by a particle in a non-linear inertial Alfvén wave propagating in a sheared flow as a function on initial phase for the following parameters: $B = B_x$, $V_A = 0.5c$, $a = 0.25$, $k_z = 0.025$, $y_s = -5$ (negative y_s is needed to have a negative shear; for positive y_s there is no acceleration), initial energy $\gamma_0 = \sqrt{2}$, initial momentum is directed along y axis. Upper curve corresponds to the case of shear shear flow and an inertial Alfvén wave, lower curve is the case without shear. Fig. 5 shows that particle indeed can gain large energies in a sheared flow: *most of the energy gain is due to motion in sheared electric field and not due to wave surfing: the wave mostly provides a drift velocity along the shear*. Without a wave, particle just executes gyrational motion near the point $y = 0$.

Another related type of acceleration in strong waves should be mentioned. In a strong inertial Alfvén wave propagating across magnetic field, fluctuating magnetic field of the wave δB_x at some wave phases reduces total magnetic field, so that total electric field (which is a sum of wave electric field and drift-induced field) may become larger than the total magnetic field. In this case, there exists a reference frame where the magnetic field is zero and only electric field is present, so that particles will experience strong acceleration. This type of acceleration is similar to surfing acceleration in strong electrostatic (upper hybrid) waves [49]. Since both charges of particles are accelerated in opposite direction, such mechanism cannot be responsible for UHECRs, see appendix A. For the parameters of our simulations condition $E < B$ is always satisfied.

B. Stage 2: large Larmor radius

When the Larmor radius becomes comparable to shear scale particle dynamics changes qualitatively. As we show below [see also 34], in case of narrow shear layers, when Larmor radius becomes comparable to shear scale, particle motion becomes unstable even for homogeneous flow, without perturbing inertial Alfvén wave.

The easiest way to consider motion of a test particle in such a case is using Hamiltonian

formalism. Let's assume that magnetic field is in the x-direction and that there is a shear velocity along z with $v_z(y) = \beta(y)c$ (Fig. 2) and transform to the frame where $v(0) = 0$. Hamiltonian of a particle in a sheared flow, $H = \sqrt{(mc^2)^2 + c^2(\mathbf{P} - e\mathbf{A}/c)^2} + e\Phi$, where $\mathbf{P}$ is generalized momentum, $\mathbf{A}$ is vector potential and Φ if electric potential, can be written as

$$H = mc^2 \left(\sqrt{1 + \frac{p_y^2}{m^2c^2} + \frac{Z^2\omega_B^2(Y_g - y)^2}{c^2}} + \frac{eZ\Phi}{mc^2} \right) \tag{34}$$

where p_y is momentum along y and $Y_g = p_z/m\omega_B$ is y coordinate of the guiding center. For linear shear the Hamiltonian is

$$H = mc^2 \left(\sqrt{1 + \frac{p_y^2}{m^2c^2} + \frac{Z^2\omega_B^2(Y_g - y)^2}{c^2}} + \frac{Z\omega_B \eta y^2}{2c^2} \right) \tag{35}$$

with the corresponding equations of motion

$$\partial_t y = \frac{p_y/m}{\sqrt{1 + \frac{p_y^2}{m^2c^2} + \frac{Z^2\omega_B^2(Y_g-y)^2}{c^2}}}$$

$$\partial_t p_y = -y\eta Z\omega_B m + \frac{(Y_g - y)Z^2\omega_B^2 m}{\sqrt{1 + \frac{p_y^2}{m^2c^2} + \frac{Z^2\omega_B^2(Y_g-y)^2}{c^2}}} \tag{36}$$

Let us assume that center of gyration is at $Y_g = 0$. After dimensionalizing, $p_y/mc \to p_y$, $y \to cy/Z\omega_B$, $t \to \omega_B t$, $\eta \to \eta\omega_B$, Eq. (36) becomes

$$\partial_t y = \frac{p_y}{\sqrt{1 + p_y^2 + y^2}}$$

$$\partial_t p_y = -\frac{y}{\sqrt{1 + p_y^2 + y^2}} - y\eta \tag{37}$$

From conservation of energy $\gamma_0 = \sqrt{1 + p_y^2 + y^2} + \eta y^2/2$, we find that the turn-around point, where $p_y = 0$ is at $y_{max} = \sqrt{2}\sqrt{1 + \gamma_0\eta + \sqrt{1 + 2\gamma_0\eta + \eta^2}}/\eta$. In addition, there exists a critical trajectory, so that as time goes to infinity a particle moves with constant velocity along z axis. In this case $\partial_t p_y = 0$ and we find $y_{max} = \sqrt{1/\eta^2 - 1}$. Equating the two expressions for y_{max} we find critical values of shear

$$\eta_{crit} = \sqrt{\gamma_0^2 - 1} - \gamma_0 \sim -\frac{1}{2\gamma_0} \quad \text{for } \gamma_0 \gg 1 \tag{38}$$

and $y_{max,crit} = \sqrt{2\beta_0/(1 - \beta_0)}$, where $\beta_0 = \sqrt{1 - 1/\gamma_0^2}$. Thus, for $\eta < \eta_{crit} < 0$, orbits are unbound and energy growth exponentially. In the limit $\gamma_0 \gg 1$ this occurs when the shear scale $L_V = c/V'$ is half of gyro-radius, $L_V = c\gamma_0/2\omega_B$.

Particle trajectories can be found in quadratures:

$$t = \int 1/\sqrt{1 - \frac{4(1+y^2)}{(2\gamma_0 - y^2\eta)^2}} dy, \tag{39}$$

(see Fig. (3)). In the non-relativistic limit equations of motion can be integrated exactly,

$$y = r_L \cos Z\omega_B \sqrt{1 + \eta/Z\omega_B}t, \; z = -\frac{r_L}{\sqrt{1 + \eta/Z\omega_B}} \sin Z\omega_B \sqrt{1 + \eta/\omega_B}t \tag{40}$$

This clearly shows that for strong negative shear, $\eta < -\omega_B$, particle trajectory is unstable and its energy growth exponentially. For positive shear, $\eta > 0$, particle motion is stable. Thus, when measured in term of particle gyration frequency ω/γ_0, critical shear reduces from -1 in the non-relativistic limit to $-1/2$ in the ultra-relativistic limit.

Similar results may be obtained numerically for velocity profile $V_z \propto \tanh(y/y_s)$. This case has an advantage over the linear profile since condition $E < B$ is satisfied everywhere. For any given γ_0 there is a critical value of $y_{s,crit} < 0$, so that for $y_{s,crit} < y_s < 0$ particle trajectories are unstable, see Fig. 4.

Energy gain occurs on time scale of $L_V/c\gamma_0$, which for strong shear is of the order of relativistic Larmor frequency. Thus, in this case *acceleration rate reaches the absolute theoretical maximum.*

This acceleration mechanism can be contrasted with shock acceleration, in which case acceleration stops when particle Larmor radius becomes of the order of system size. In contrast, inductive acceleration become more efficient when particle is unconfined.

VI. SPECTRUM OF ACCELERATED PARTICLES

The acceleration mechanism proposed here requires a presence of pre-accelerated seed of particle with large Larmor radius. Pre-acceleration mechanism may operate outside of the jet; radial drift then may "pull" particles inside a jet. Since magnetic field at the periphery is relatively small (*e.g.* falling off as $1/r$), even relatively small energy particle would have large Larmor circle and will experience fast radial drift. This can serve as an injection mechanism if at the base of the jet, near the central galaxy, there is a population of pre-accelerated particles.

In a steady state, the total particle energy gain is determined by the local electric potential, which, in turn, depends on magnetic field and velocity distribution. These are highly

uncertain functions for the AGN jets. As an alternative model problem we consider temporal evolution of distribution of pre-accelerated particles injected into jet at initial time and evolving due to gradient drift in sheared flow. Assuming $\gamma \gg 1$, the evolution of the distribution function ($f = \frac{dn}{d\gamma}$) in the rest frame is described by

$$\partial_t f + \partial_\gamma \left(\partial_t(\gamma) f \right) = S \tag{41}$$

where S is density of sources. Assuming impulsive injection of seed population, integration along characteristics (30) gives a solution

$$f(\gamma, t) = f_0(\gamma_0(\gamma, t), t = t_0) \left(\frac{\gamma_0}{\gamma} \right)^2 \tag{42}$$

If the initial injection spectrum is power-law, $f_0 \propto 1/\gamma_0^p$, then

$$
\begin{aligned}
f(\gamma, t) &\propto \frac{1}{\gamma^p} \left(1 + \gamma \left(\frac{t}{\tau_0} \right)^2 \right)^{p-2} \\
&\sim \gamma^{-2}, \quad \text{for } \gamma t^2 / \tau_0^2 \gg 1
\end{aligned}
\tag{43}
$$

Thus, for $p > 2$ the spectrum flattens with time.

The hardest spectrum that can be achieved has a power law index of 2. This limiting case corresponds to unlimited acceleration in a plane-parallel geometry, which is realistically applicable to energies well below the total available potential. At highest energies the final spectrum will depend on the distribution of pre-accelerated particles with respect to the electric potential and, in case of contribution from many sources, on distribution of total potentials.

Relation between the observed spectrum and spectrum at the source is not simple and depends on source distribution and (poorly constrained) extragalactic magnetic fields . Since high power AGNs are located at the edge of the GZK sphere, a flat spectrum at the source, with p approaching 2, seems to be required in order to account for AGASA observations of UHECRs above the ankle [2, 50]. We note however that in the high energy region we discuss here currently there seems to be a disagreement between the AGASA ground array ([51]) and the HiRes fluorescence detector ([52]). Much larger experiments such as Auger, Extreme Universe Space Observatory (EUSO), and Orbiting Wide-angle Light-Collectors (OWL) will put much better constraints on the injection spectrum.

VII. ASTROPHYSICAL VIABILITY

One of the key observational test of UHECRs origin is the identification of the transition from the galactic to extragalactic components. The two competing models are the "ankle scenario" [see, *e.g.* , 53, for a general discussion of the transition], when the transition is identified with the intersection of a steep galactic and flat extragalactic spectra, and the "dip" scenario, when the transition is identified with the "second knee" [see, *e.g.* , 54]. Our model is consistent with the dip scenario as we discuss below.

Chemical composition In our model the EGCRs and the GCRs have different spatial and astrophysical origin. We assume however that the mechanism driving the pre-accelerated component at the acceleration cite of UHECRs is also at play in our galaxy. From a pool of pre-accelerated particles, the ones with the highest rigidity are accelerated most efficiently. Thus, the population of pre-accelerated CRs is a mixture of heavy and light nuclei, the drift mechanism will preferably accelerate protons. Our model thus predicts an increase in proton over heavy elements as the energy of the UHECR increases. Such trends have apparently been observed in the composition of UHECRs with energies between $\sim 5 \times 10^{17}$ eV ("second knee") and 10^{19} eV and extending to energies above $10^{19.3}$ eV ([65, 66]). [See [67] for a discussion of systematic differences between different measurements and how it limits our knowledge of the composition of CRs of the highest energies.]

Injection spectrum The hardest injection spectrum the model can account for is power law index of 2. The dip models generally prefer softer spectra, with index $2.5-2.7$; such softer spectrum can be achieved both due to spread out distribution of pre-accelerated particles with respect to the total potential inside a given jet and by a combination of contribution from many sources with different potential drops [54, 68]. For the case of injection spectrum with index 2 the distribution of the sources with respect to maximum acceleration energy E_{max} required to explains the observational data is $dn/dE_{max} \propto^E_{max} -1.5$ [68]. The model also naturally provides a lower cut-off to the injection spectrum (see below).

Density of sources: isotropy and clustering of UHECRs. We associate acceleration cites of UHECRs with powerful FRII galaxies. Assuming proton composition, to account for energies above 10^{20} eV the source luminosity should be no less than 10^{46} ergs/s (see §2). Assuming $\sigma \sim 1$, this translates into a limit on a total power of a jet. The total jet power, as well as power in electromagnetic component are not straightforward to estimate.

Rawlings and Sauders [55] give estimates of jet power in FR II galaxies based on assumption of equipartition between the magnetic field and relativistic electrons and expansion dynamics of hot spots. According to this *minimum* energy estimate, powers of FR II galaxies reach $10^{45} - 10^{47}$ erg/sec, while FR I are an order of magnitude less powerful. This limits the possible acceleration sites to FR II radio galaxies which are typically far apart. The power in strongly beamed sources, like flat spectrum radio quasar, are harder to estimate: radiative modeling [56] gives estimates comparable to FR II galaxies, up to 10^{49} erg/s. In any case, requirements on luminosity (and assumption of high proton content in UHECRs) *excludes* prominent low power nearby sources, like FR I radiogalaxy Cen A, nearest AGN M87 and starburst galaxy M82. We favor high power radio galaxies at intermediate distances as sources of UHECRs.

The observed number density of highest power sources is a power law in energy, with sources of $L \sim 10^{45} erg/s$ having density $\sim 10^{-6} Mpc^{-3}$. This is smaller by approximately an order of magnitude than the density required to produce the small scale clustering, $\sim 10^{-5} Mpc^{-3}$, [72], but, first, the inferred density has a large uncertainty and, second, the intrinsic electromagnetic luminosity is definitely higher than the observed radiative one.

Shape of GZK cut-off. Small spacial density of sources also has a clear prediction for the shape of the GZK cut-off [54]. Our model predicts very steep GZK cutoff.

Total energy budget. The model naturally avoids the energy budget problem posed by the steep required injection spectrum (in which case total energy density is determined by a somewhat arbitrary lower energy cut-off). In the proposed mechanism, below some limiting energies particles just do not leave the jet. Though details depend on jet properties, requiring that a cosmic ray crosses a 10 kpc jet over acceleration of jet length of 100 kpc, one can estimate $E_{min} \sim 10^{16}$ eV.

High energy photon and neutrino traces. If high power, fairly distant AGNs are sources of UHECR, one may expect that as particle travel towards the observer they initiate electromagnetic cascades due to photo-pion production on CMB. Most of the energy of electromagnetic cascades ends up in photons in the GeV-TeV range. If propagation is almost rectilinear, one may expect an increase of high energy photon flux towards a source at a level of $\sim 10^{-14}$ cm^{-2} s^{-1} [75]. This flux can be (barely) detected by Cherenkov experiments like HESS. Deflection of UHECR in localized regions of high magnetic field, associated, for example, with supergalactic plane may easily make this flux to be distributed over large area

of the sky. To produce considerable deflection a magnetized sheath of thickness of 1 Mpc with magnetic field of the order of 10^{-6} is required [76]. This may also explain non-detection of UHECR towards a particular AGN. Finally, significant neutrino fluxes can be generated if protons are accelerated up to 10^{21} eV energies [77]. We note however that the induced 10^{18} eV neutrinos are below the currently advertised threshold for EUSO, OWL and ANITA, and most of the potential events will go undetected [78].

VIII. DISCUSSION

In this work we have considered a new mechanism of acceleration of UHECRs to energies above the ankle by inductive electric fields in sheared flows. The main points are:

(i) *In a sheared flow protons are at a maximum electric potential energy if* $\mathbf{B} \cdot \nabla \times \mathbf{v} < 0$, so that kinetic drift motion along the shear will lead to fast energy gains. If a jet is generated by rotating system of black hole-accretion disk with the velocity falling off with cylindrical radius, then the quantity $\mathbf{B} \cdot \nabla \times \mathbf{v}$ will be determined by the product $\mathbf{B} \cdot \Omega$ at the source, where Ω is the angular velocity of the black hole-accretion disk system driving the jet.

Radial drift motion may occur if a jet is inhomogeneous along its axis, so gradient drifts will lead to energy gains. Alternatively, one may imagine that the toroidal magnetic field is perturbed azimuthally and is sheared by differential velocity flow. This will generate non-axisymmetric poloidal magnetic field, which would result in radial drift. Finally, particle diffusion, resonant or due to field line wondering, may lead to radial particle motion. In any case, a particle must cross the magnetic field lines in order to gain energy.

(ii) Since drift velocity is an increasing function of energy, *acceleration rate is also an increasing function of energy*. Thus, from a pre-accelerated population this mechanism will pick up the highest energy particles and boost their energy further. In addition, since energy gain is independent of the direction of the drift, pre-accelerated population may be located outside of the jet and be pulled-in by gradient drift. Pre-acceleration may be achieved, for example, by non-linear shock acceleration in supernova and/or cluster shocks [79].

(iii) After a particle has crossed a substantial fraction of the total potential available in the system, its Larmor radius becomes comparable to the flow scale. In this case exponential acceleration may proceed without gradient drift. As a result, the *acceleration rate reaches the theoretical maximum (acceleration on time scale of one gyration)* and finally a particle

can leave the system.

(iv) Since acceleration is fastest for highest rigidity particles, from a population of a pre-accelerated particles with mixed composition, *particles with smallest charge – i.e. protons – are accelerated most efficiently.* We thus predict a dominance of protons over heavy nuclei for energies above the ankle.

(v) Drift acceleration can also produce hard spectra, which are required if sources are located at the edge of the GZK sphere. We have also calculated the spectrum of UHECRs assuming impulsive injection of pre-accelerated particles with a steep power law spectrum. *Due to inductive acceleration the energy spectrum flattens and reaches asymptotically a power law index of 2.*

The best astrophysical location for operation of the proposed mechanism is *cylindrically collimated*, high power AGN jets. The proposed mechanism cannot work in spherically (or conically) expanding outflows since in this case a particle experiences polarization drift, which is a *first order* in Larmor radius, due to the fact that in the flow frame magnetic field decreases with time. For a constant velocity flow this drift is always against the electric field (for a positively charged particle) and lead to the decrease of energy on time scale $R/(c\Gamma)$, where R is a distance from the central source and Γ is the Lorentz factor of the flow. [A flow must acceleration faster than $\Gamma \sim r$ in order to beat this polarization drift.] Comparing with acceleration time scale (32), and assuming $L_E \sim L_B \sim R/\Gamma$, we conclude that the expansion time scale is shorter than the acceleration time scale by a factor $\sim \sqrt{Rc/\gamma\Gamma\omega_B} \gg 1$. Thus, in spherically expanding flows adiabatic losses always dominate over regular energy gain due to drift motion: the proposed mechanism would fail then. On theoretical grounds, AGN jets (or at least their cores) may indeed be asymptotically cylindrically collimated [44]. Observations of large scale jets, *e.g.* Pictor A, do show jets that seem to be cylindrically collimated on scales of tens of kiloparsec.

In cylindrically collimated parts of the jet acceleration can happen from sub-parsec to hundreds of kiloparsec scales: as long as the motion of the jet is relativistic the total electric potential remains approximately constant. Thus, UHECRs need not be accelerated close to the central black hole where radiative losses are important [*cf.* 11]. After a jet has propagated parsecs from the central source radiative losses become negligible, see Eq. 6.

Another constraint on the mechanism comes from the requirement that in order to produce radial kinetic drift the jet magnetic field should be inhomogeneous along the axis.

Though shocks provide possible inhomogeneity of magnetic field (δ-function inhomogeneity on the shock front), we disfavor shock since particles are advected downstream and cannot drift large distances along shock surface. In a gradual inhomogeneity a particle drifts orthogonally to the field gradients and thus generally will remain in the region of inhomogeneous fields. [One may imagine a hybrid model, where scattering brings a particle back to shock front, similar to Eichler's model of shock acceleration near Earth bow shock, [20]]. Extragalactic jets are expected to have axial inhomogeneities, both due to non-stationary conditions at the source and due to propagation of compression and rarefaction waves generated at the jet boundary via interaction with surrounding plasma.

IX.   PREDICTIONS

Our model has a number of clear predictions, some of which are related to astrophysical association of acceleration sites of UHECRs with AGN jets [2] and some are specific to the model: (i) one needs a relatively powerful AGN, with luminosity $\geq 10^{46}$ erg/sec. This limits possible sources to high power sources like FR II radiogalaxies, radio loud quasars and high power BL Lacs (flat spectrum radio quasars). Powerful AGNs are relatively rare and far apart, so that a steep GZK cut-off corresponding to large source separation should be seen. (ii) UHECRs come from sources with low spacial density. This may be reflected in the distribution of arrival directions. (iii) Extragalactic UHECRs should be dominated by protons. (iv) Depending on "extra-galactic seeing conditions" arrival directions of UHECRs may point to their sources, though complicated magnetic field structure may erase this correlation. In addition, the fact that only flows with negative shear can accelerate protons implies that only approximately half of such AGNs can be sources of UHECRs (this assumes that the AGN central engine - black hole or an accretion disk - is dominated by large scale, dipolar-like magnetic field).

Canada.

---

[1] Blandford, R. D., 2000, Physica Scripta Volume T, 85, 191

[2] Olinto, A. V., 2000, Phys. Rep., 333, 329

[3] Ostrowski, M., 2000, MNRAS, 312, 579

[4] Torres, D. F. and Anchordoqui, L. A., 2004, Reports of Progress in Physics, 67, 1663

[5] Parizot, E. 2005, in New Views on the Universe, Proc. of the Vth Rencontres du Vietnam (Hanoi, 2004), astro-ph/0501274

[6] Kirk, J. G., Duffy, P., 1999, Nuclear Physics, 25, 163

[7] Baring, M. G., 2004, Nuclear Physics B, 136, 198

[8] Niemiec, J. and Ostrowski, M., 2004, Astrophys. J. , 610, 851

[9] Wick, S. D. and Dermer, C. D. and Atoyan, A., 2004, Astroparticle Physics, 21, 125

[10] Allard, D., *et al.* , 2005, [astro-ph/0505566]

[11] Levinson, A., 2000, Physical Review Letters, 85, 912

[12] Blasi, P. and Epstein, R. I. and Olinto, A. V., 2000, ApJ Lett., 533, 123

[13] Arons, J., 2003, Astrophys. J. , 589, 871

[14] Bell, A. R., 1992, MNRAS, 257, 493

[15] van Putten, M. H. P. M., 1996, ApJ Lett., 467, 57

[16] Ouyed, R. and Pudritz, R. E., 1997, Astrophys. J. , 484, 794

[17] Komissarov, S. S., 1999, MNRAS, 308, 1069

[18] Webb, G. M. and Axford, W. I. and Terasawa, T., 1983, Astrophys. J. , 270, 537

[19] Jokipii, J. R., 1982, Astrophys. J. , 255, 716

[20] Eichler, D., 1981, ApJ, 244, 711

[21] Berezhko, E. G., & Krymskii, G. F. 1981, Sov. Astr. Lett. 7, 352

[22] Jokipii, J.R., & Morfill, G.E. 1990, ApJ, 356, 255

[23] Rieger, F. M. and Duffy, P., 2004, Astrophys. J. , 617, 155

[24] Lesch, H., Birk, G.T., Schopper, R., 2002, Plasma Phys. Control. Fusion, 44, B1-B9

[25] Kronberg, P. P. and Colgate, S. A. and Li, H. and Dufton, Q. W. , 2004, ApJ Lett., 604, 77

[26] Berezinsky, V. and Gazizov, A. Z. and Grigorieva, S. I. , 2006, Phys. Rev. D, 74, 043005

[27] Arons, J. and Scharlemann, E. T., 1979, Astrophys. J. , 231, 854

[28] Lovelace, R. V. E., 1976, Nature, 262, 649

[29] Hillas, A. M., 1984, ARAA, 22, 425

[30] Kennel, C. F. & Coroniti, F. V. 1984, ApJ, 283, 710

[31] Medvedev, M. V., 2003, Phys. Rev. E , 4, 045401

[32] Lyutikov, M., Pariev, V.I., & Gabuzda, D., MNRAS, in press [astro-ph/0406144]

[33] Gaisser, T. K. and Stanev, T., 2005, astro-ph/0510321

[34] Ganguli, G. and Lee, Y. C. and Palmadesso, P. J., 1988, Physics of Fluids, 31, 823

[35] Cai, D. and Storey, L. R. O. and Neubert, T., 1990, Physics of Fluids B, 2, 75

[36] Ganguli, G., 1995, Physics of Plasmas, 4, 1544

[37] Blandford, R.D., & Znajek, R.L. 1977, MNRAS, 179, 433

[38] Blandford, R.D., & Payne, D.G. 1982, MNRAS, 199, 883

[39] Begelman, M.C., Blandford, R.D., & Rees, M.J. 1984, Rev. Mod. Phys., 56, 255

[40] McKinney, J. C. and Gammie, C. F., 2004, Astrophys. J. , 611, 977

[41] Lyutikov, M., Pariev, V.I., & Blandford, R.D., 2003, Astrophys. J. , 597, 998

[42] Blandford, R.D. 2002, in Lighthouses of the Universe: The Most Luminous Celestial Objects and Their Use for Cosmology , ed. R. Sunyaev, (Berlin: Springer-Verlag), p. 381

[43] Lyutikov, M., Blandford, R.D., 2003, astro-ph/0312347

[44] Heyvaerts, J. & Norman, C. 2003, ApJ, 596, 124

[45] Henri, G. and Pelletier, G., 1991, ApJ Lett., 383, L7

[46] Chiaberge, M. and Celotti, A. and Capetti, A. and Ghisellini, G. , 2000, AAP, 358, 104

[47] Giroletti, M. et al. , 2004, Astrophys. J. , 600, 127

[48] Clemmow, P. C., 1974, Journal of Plasma Physics, 12, 297

[49] Katsouleas, T. & Dawson, J. M., 1983, Phys. Rev. Lett., 51, 392

[50] Olinto, A. V., 2004, [astro-ph/0404114]

[51] Takeda, M., et al. , 2002, ApJ, 522, 225

[52] Abbasi, R. U., et al. , 2005, Astropart. Phys., 23, 157

[53] DeMarco, D. and Stanev, T., Phys. Rev. D, 72, 081301

[54] Aloisio, R. and Berezinsky, V. and Blasi, P. and Gazizov, A. and Grigorieva, S. and Hnatyk, B., 2006, astro-ph/0608219

[55] Rawlings, S. and Saunders, R., 1991, Nature (London) , 349, 138

[56] Ghisellini, G., 2004, Nuclear Physics B Proceedings Supplements, 132, 76

[57] Rachen, J. P. and Biermann, P. L., 1993, AAP, 272, 161

[58] Tavecchio, F. and Maraschi, L. and Sambruna, R. M. and Urry, C. M., 2000, ApJ Lett., 544, 23

[59] Ostrowski, M. and Siemieniec-Ozieblo, G., 2002, AAP, 386, 829

[60] DeMarco, D., Blasi, P., & Olinto, A. 2003, Astropart. Phys., 20, 53

[61] Berezinsky, V. and Gazizov, A. Z. and Grigorieva, S. I. , 2005, Physics Letters B, 612, 147

[62] Deligny, O., Letessier-Selvon, A., & Parizot, E. 2004, Astropart. Phys. 21, 609

[63] Aloisio, R. and Berezinsky, V., 2004, Astrophys. J. , 612, 900

[64] Stanev, T., Seckel, D., & Engel, R. 2003, Phys. Rev. D, 68, 103004

[65] Shinozaki, K., et al. AGASA collaboration, in the Proceedings of the 28th International Cosmic Ray Conference in Tsukuba, Japan

[66] Ave et al. 2003, Astroparticle Physics, 19, 61

[67] Watson, A. A. 2004, Nucl. Phys. B, 136, 290

[68] Kachelrieß, M. and Semikoz, D. V., 2006, Physics Letters B, 634, 143

[69] Kronberg, P. P. 1994a, Rep. Prog. Phys., 57, 325

[70] Kronberg, P. P. 1994b, Nature, 370, 179

[71] Uchihori, Y., *et al.* , 2000, Astroparticle Physics 13, 151

[72] Blasi, P. and de Marco, D., 2004, Astroparticle Physics, 20, 559

[73] Sigl, G. 2004, Acta Phys. Polon. B35 1845 [astro-ph/0404074]

[74] Alvarez-Muńiz, J., Engel, R., & Stanev, T. 2002, ApJ, 572, 185

[75] Ferrigno, C. and Blasi, P. and de Marco, D., 2004, Nuclear Physics B, 136, 191

[76] Sigl, G. and Miniati, F. and Enßlin, T. A., 2004, Nuclear Physics B, 136, 224

[77] Waxman, E., & Bahcall, J. 1999, Phys. Rev. D, 59, 023002

[78] Halzen, F., & Hooper, D. 2002, Rep. Prog. Phys., 65, 1025

[79] Bell, A. R. and Lucek, S. G., 2001, MNRAS, 321, 433

[80] Raadu, M. A., 1989, Phys. Rep., 178, 25

[81] Boldt, E. and Ghosh, P., 1999, MNRAS, 307, 491

[82] Waxman, E., 2004, Astrophys. J. , 606, 988

[83] Landau, L. D. and Lifshitz, E. M., 1959, Fluid mechanics, Oxford: Pergamon Press, 1959

[84] Generally, $\nabla \times \mathbf{B} \neq 0$ due to advective current $\sim (\nabla \cdot \mathbf{E})\mathbf{v}$. In other words, $B/sqrt{1 - (v/c)^2}$ is constant, but not the value of magnetic field itself.

[85] Keeping the $\mathbf{v} \cdot (\nabla \times \mathbf{B})$ term in Eq. (14) and assuming force-free balance $\mathbf{E} \operatorname{div}\mathbf{E} + \mathbf{j} \times \mathbf{B} = 0$, we find $\mathbf{j} = \operatorname{div}\mathbf{E}\,\mathbf{v}$, which gives $\Delta\Phi = \frac{(\mathbf{B} \cdot \nabla \times \mathbf{v})}{c(1 + (v/c)^2)}$.

APPENDIX A: IMPOSSIBILITY OF ACCELERATION OF UHECRS IN DC ELECTRIC FIELDS

Acceleration by DC electric fields, when there is component of electric field along magnetic field or when $E > B$, is fast and very efficint way of gaining energy. On the other hand, in this appendix we argue that *UHECRs cannot be accelerated by DC electric fields*. There are two reasons. First, if we have a gap (region where there is an uncompensated electric field parallel to magnetic field), any lepton will undergo acceleration and after passing a potential drop of the order of $10^6 - 10^8$ eV will produce a pair, *e.g.* through inverse Compton effect or curvature emission. The secondary pairs will similarly be accelerated, producing an electromagnetic cascade that will short out the initial DC electric field. Secondly, even if one manages to create an extremely photon-clean surrounding with straight magnetic fields, the electric field will accelerate both signs of charges, producing field-aligned current. The magnetic field, associated with these currents would have prohibitively large energy as we show below.

Consider a one dimensional double layer with potential difference Φ_{tot} that can freely emit particles from each end. To account for possible effects of rotation and associated charge density we introduce Goldreich-Julian density n_{GJ} in the potential equation The governing equations are

$$\partial_z^2 \phi = 4\pi(n_i e_i - n_e e + n_{GJ} e)$$

$$j_e = e n_e v_e = const$$

$$j_i = e_i n_i v_i = const$$

$$\left(\frac{1}{\sqrt{1 - v_e^2/c^2}} - 1 \right) m_e c^2 = e\phi$$

$$\left(\frac{1}{\sqrt{1 - v_i^2/c^2}} - 1 \right) m_i c^2 = e_i(\Phi_{tot} - \phi) \tag{A1}$$

where z is the coordinate along the electric field, n and e are density and charges, j is the

current density, v is velocity of two species. Thus

$$v_e = \frac{\sqrt{\phi}\sqrt{2m_ec^2/e + \phi}}{m_ec^2/e + \phi}c$$

$$v_i = \frac{\sqrt{\Phi_{tot} - \phi}\sqrt{2m_ic^2/e_i + \Phi_{tot} - \phi}}{m_ic^2/e_i + \Phi_{tot} - \phi}c \tag{A2}$$

Putting into potential equation, we find

$$\phi'' = \frac{4\pi}{c}\left(n_{GJ}e - \frac{j_e(e\phi + m_ec^2)}{\sqrt{e\phi(e\phi + 2m_ec^2)}} + \frac{j_i(m_ic^2 + e_i(\Phi_{tot} - \phi))}{\sqrt{e_i(\Phi_{tot} - \phi)(2m_ic^2 + e_i(\Phi_{tot} - \phi))}}\right) \tag{A3}$$

which can be integrated once. The solution of (A3) should satisfy the boundary conditions: at $\phi(z = 0) = 0$, $\phi'(z = 0) = 0$, $\phi(z = H) = \Phi_{tot}$, $\phi'(z = H) = 0$ (there is no electric field on each end). Thus the problem is an eigenvalue problem on currents. We find

$$\frac{j_ie}{j_ee_i} = \sqrt{\frac{2m_ec^2/e + \Phi_{tot}}{2m_ic^2/e_i + \Phi_{tot}}} + \frac{n_{GJ}e_ic}{j_i\sqrt{2m_ec^2/(e\Phi) + 1}} \tag{A4}$$

which generalizes the relativistic Child's law [80], see also [27]. Equation for ϕ' then becomes

$$\frac{\phi'^2}{2} = \frac{4\pi j_e}{c}\left(\sqrt{2m_ec^2/e + \Phi_{tot}}\left(\sqrt{\Phi_{tot}} - \frac{\sqrt{\Phi_{tot} - \phi}\sqrt{2m_ic^2/e_i + \Phi_{tot} - \phi}}{\sqrt{2m_ic^2/e_i + \Phi_{tot}}}\right)\right.$$

$$\left.-\sqrt{\phi}\sqrt{2m_ec^2/e + \phi} - \frac{n_{GJ}ec}{j_e}\left(\Phi_{tot} - \phi - \sqrt{\frac{\Phi_{tot}(\Phi_{tot} - \phi)(2m_ic^2/e_i + \Phi_{tot} - \phi)}{2m_ic^2/e_i + \Phi_{tot}}}\right)\right) \tag{A5}$$

dimensionalizing $m_e = \mu m_i$, $\phi \to \phi\Phi_{tot}$, $\Phi_{tot} = \gamma_0 m_ic^2/(Ze)$ (γ_0 has a meaning of a maximal Lorentz factor that ions can reach), $n_{GJ} \to \beta_{GJ}j_i/(ec)$ and $z \to \gamma_0^{3/4}\sqrt{\frac{m_ic^3}{4\pi eZj_i}}z$, equation for ϕ' becomes

$$\frac{\phi'^2}{2} = -\sqrt{\gamma_0 + 2} + \sqrt{(1 - \phi)(2 + \gamma_0(1 - \phi))} + \sqrt{\frac{(\gamma_0 + 2)\phi(2Z\mu + \gamma_0\phi)}{\gamma_0 + 2Z\mu}} -$$

$$\beta_{GJ}\sqrt{\gamma_0}\phi\left(1 - \sqrt{\frac{2Z\mu + \gamma_0\phi}{\phi(\gamma_0 + 2Z\mu)}}\right) \tag{A6}$$

In the limit of highly relativistic ions, $\gamma_0 \gg 1$, this becomes

$$\frac{\phi'^2}{2} = \frac{\phi + (Z + \beta_{GJ})\mu(1 - \phi)}{\sqrt{\gamma_0}} \approx \frac{\phi}{\sqrt{\gamma_0}} \tag{A7}$$

This determine the length of the double layer in dimensionless units.

$$z = \sqrt{2}\gamma_0^{1/4} \tag{A8}$$

Returning to dimensional notations we find that the maximum potential a double layer of size R, carrying a current I (so that $j_i \sim I/2R^2$, assuming that the width of the current layer is of the order of its length) may have is

$$\Phi_{tot} = \sqrt{2\pi}\sqrt{\frac{Im_ic}{Ze}} \qquad (A9)$$

The maximum energy is then

$$\mathcal{E}_{max} \sim \sqrt{Im_icZe} \qquad (A10)$$

Since $I < c\sqrt{E_{tot}/R}$, where E_{tot} is total energy in a system,

$$\mathcal{E}_{max} \leq \sqrt{m_ic^2Ze}\left(\frac{E_{tot}}{R}\right)^{1/4} \leq 10^{15}\mathrm{eV}\sqrt{Z}\left(\frac{E_{tot}}{10^{60}\mathrm{erg}}\right)^{1/4}\left(\frac{R}{10\mathrm{kpc}}\right)^{-1/4} \qquad (A11)$$

Thus, the maximum energy achievable by a particle scales only as $E^{1/4}$ (c.f. with maximum energy achievable in inductive field, $\propto L^{1/2}$, Eq. (4)). Even the largest energy reservoirs, lobes of radio galaxies, cannot provide large enough potential for DC acceleration of UHE-CRs. For magnetars with $B \sim 10^{15}$ G and $R \sim 10^6$ cm estimate (A11) gives $\mathcal{E}_{max} \sim 1.6\times10^{16}$ eV, while for supermassive blackholes with $B \sim 10^4$ G and $R \sim 10^{13}$ cm, $\mathcal{E}_{max} \sim 1.6 \times 10^{14}$ eV. This excludes the possibility of UHECR acceleration by DC electric fields in astrophysical environment.

There is only one way to circumvent this argument: acceleration region must be really devoid of any plasma [as, for example, suggested by 11, 81, in the immediate surrounding of dead quasars].

APPENDIX B: CAN GRB SHOCKS ACCELERATE UHECR?

Simple estimates (4) shows that only very luminous sources have enough potential to acceleration UHECR. GRBs, with peak luminosity of the order of 10^{51} erg/s and total potential $\Phi_{GRB} \sim 4 \times 10^{22}$ V, are then prime suspects [eg 82]. Still, we disfavor this possibility for the following reasons. Internal shocks, where UHECRs are supposed to be accelerated, are short transient events occurring at distances $\sim 10^{12} - 10^{13}$ cm. In order to overcome radiative losses, from Eq. (6) it follows that Lorentz factor should be $\Gamma \geq 300$. The first problem is that for spherically expanding ultra-relativistic flows the available potential is smaller than (4) by a factor $1/(\Gamma\Delta\theta) \ll 1$, since particle can cross sideways only a distance

$\sim R/\Gamma$. To see this, consider a conically expanding flow with total luminosity L and opening solid angle $\Delta\Omega = \pi\Delta\theta^2$. [All the relations below apply, roughly, both to large scale and small scale magnetic fields.] If b is the magnetic field in the flow rest-frame, using (3) we can write the rest-frame magnetic field as

$$b \sim \sqrt{\frac{\sigma}{1+\sigma}}\sqrt{\frac{L}{c}}\frac{1}{\Gamma\Delta\theta R} \tag{B1}$$

The available potential in the rest frame is then

$$\Phi_{rest} \sim b\frac{R}{\Gamma} \sim \sqrt{\frac{\sigma}{(1+\sigma)}}\frac{1}{\Gamma^2\Delta\theta}\sqrt{\frac{L}{c}} \tag{B2}$$

while in the laboratory frame it is

$$\Phi_{lab} \sim \Gamma\Phi_{rest} \sim \Gamma b\frac{R}{\Gamma} \le \sqrt{\frac{\sigma}{(1+\sigma)}}\frac{1}{\Gamma\Delta\theta}\sqrt{\frac{L}{c}} = 3.6\times10^{21}\,\mathrm{V}\sqrt{\frac{\sigma}{1+\sigma}}\left(\frac{\Gamma\Delta\theta}{30}\right)^{-1}\left(\frac{L}{10^{51}\mathrm{ergs}^{-1}}\right)^{1/2} \tag{B3}$$

(since both electric field and magnetic fields are larger in laboratory frame by a factor Γ). At the time when internal shocks are supposed to occur, $\Gamma\Delta\theta \gg 1$, so that the available potential (B3) is smaller than the total potential by a factor $\Gamma\Delta\theta \sim 30$ (for $\Gamma = 300$ and $\Delta\theta \sim 0.1$). Potential (B3) is still large enough, so that sub-equipartition fields, $\sigma \ge 0.01$ are sufficient.

[In passing we note that the restriction discussed above applies only to UHECR acceleration at GRB internal shocks occurring at small distances. Since the total potential remains approximately constant as long as the expansion is relativistic, $\Gamma \ge 1$, but the available potential increases for decreasing Γ until $\Gamma \sim 1/\Delta\theta$ and remains constant after that, it is feasible that UHECRs are accelerated at later stages, when the flow becomes trans-relativistic. This cannot, though, be done neither at external shock since magnetization there is low, nor at internal shocks, since the flow becomes trans-relativistic long time after internal shocks have been dissipated.]

Secondly, and most importantly, as long as particle has not crossed *all* the available potential (B3), its Larmor radius is smaller than the size of the flow in its rest frame $r_L < R/\Gamma$. After crossing fraction ξ of the total available potential in rest frame (B2) the maximum Larmor radius becomes

$$r_L = \xi\frac{\Phi_{rest}}{b} = \xi\frac{R}{\Gamma}\,, \tag{B4}$$

In a framework of shock acceleration, if Larmor radius is smaller than the size of the system, $\xi < 1$, a particle is advected with the flow and is then subject to strong adiabatic losses, losing all the energy that it gained from acceleration process. Thus, in order to avoid adiabatic losses a particle *must* cross all the available potential so that its Larmor radius would become of the order of the flow scale and adiabatic approximation would break down. Condition (B4) is equivalent to the requirement that acceleration time scale for highest energy UHECRs is of the order of flow expansion. Thus, the paradigm of shock acceleration of UHECRs in GRBs *requires* that particles are accelerated on time scale of inverse relativistic gyro-frequency, nothing less will do. We consider this condition, though formally within the limits of shock acceleration, as a very restrictive and thus disfavor UHECRs at internal shocks in GRBs.

APPENDIX C: ELECTROMAGNETIC WAVES IN TRANSVERSELY SHEARED PLASMA

In this Appendix we consider properties of electromagnetic waves in transversely sheared cold plasma. The results presented here will server as a basis for background electromagnetic field that lead to particle acceleration. One of the key differences between our approach and previous works [34] is that *waves in transversely sheared plasma cannot be considered self-consistently in the framework of non-relativistic MHD*, since, as we showed in Section III shear introduces charge density, which is neglected by non-relativistic MHD. In addition, for perturbations propagating orthogonally to magnetic field, *inertial Alfvén waves* play a crucial role, so that induction current, which is neglected in non-relativistic MHD, is important.

Consider cold plasma composed of two species $\alpha = e, p$. Maxwell equations, continuity and equations of motions then read (in this Section we assume $c = 1$)

$$\partial_t \mathbf{B} = -\operatorname{curl} \mathbf{E}$$

$$\operatorname{curl} \mathbf{B} = 4\pi \mathbf{J} + \partial_t E$$

$$\operatorname{div} E = 4\pi \sum n_\alpha e_\alpha$$

$$\operatorname{div} B = 0$$

$$\partial_t n_\alpha + \nabla(\mathbf{v} n_\alpha) = 0$$

$$\mathbf{J} = \sum n_\alpha e_\alpha \mathbf{v}_\alpha$$

$$\partial_t \mathbf{v}_\alpha + (\mathbf{v}_\alpha \cdot \nabla)\mathbf{v}_\alpha = \frac{e_\alpha}{m_\alpha}\left(E + (v_\alpha \times \mathbf{B})\right) \tag{C1}$$

Below we assume that electrons (subscript 1) carry a charge $-e$ while positive chargers are protons with charge e.

Assume that the magnetic field is along x-axis $B_x = B_0$ and that there is sheared flow along y-direction with $V = V_z(y)$. Then, there is electric field $E_y = -V_z(y)B_0$ and corresponding charge density

$$\rho_0 = \frac{1}{4\pi}\,\mathrm{div}\,E = -\frac{1}{4\pi}V'B_0 \tag{C2}$$

Consider small fluctuations on this background $\propto \exp\{i(k_x x + k_z z - \omega t)\}$, $\mathbf{B} = \mathbf{B}_0 + \delta b$, $\mathbf{E} = \mathbf{E}_0 + \delta e$, $n_\alpha = n_0 + n_\alpha$, $\mathbf{v} = \mathbf{V} + \mathbf{v}_\alpha$. Assuming, for simplicity $k_x = 0$, perturbations are governed by equations

$$\delta b_y = -\frac{k_z e_z}{\omega}, \delta b_z = \frac{ie'_x}{\omega}, \delta b_x = -\frac{ie'_z + k_z e_y}{\omega}$$

$$i\omega e_y + 4\pi n_0 e(v_{1y} - v_{2y}) = 0$$

$$i\omega e_z - \delta b'_x = 4\pi n_0 e((n_1 - n_2)V + n_0(v_{1z} - v_{2z}))$$

$$\delta b'_z = i(k_z \delta b_y - \omega e_x)$$

$$\delta b'_y = -ik_z \delta b_z$$

$$e'_y + ik_z e_z = 4\pi e(n_1 - n_2)$$

$$-\omega n_\alpha + k_z n_0 v_{1x} - in_0 v'_{\alpha y} + k_z n_1 V = 0$$

$$\omega_{B\alpha}(e_y + \delta b_x V) + B_0\left(i\omega_D v_{\alpha y} + \omega_{B,\alpha} v_{\alpha z}\right) = 0$$

$$\omega_{B\alpha} e_z + i\left(\omega_D v_{\alpha z} + v_{\alpha y}(\omega_{B\alpha} + V')\right) = 0$$

$$e_x = \delta b_y V \tag{C3}$$

where $\omega_D = \omega - k_z V$. Eliminating $\delta \mathbf{b}$ and n_α:

$$n_\alpha = \frac{k_z v_{\alpha z} - iv'_{\alpha y}}{\omega_D} \tag{C4}$$

we derive the velocity fluctuations as

$$v_{\alpha y} = \frac{\omega_{B\alpha}\left(\omega\omega_{B\alpha}e_z - \omega_D V e'_z - i\omega_d^2 e_y\right)}{B_0 D_\alpha \omega}$$

$$v_{\alpha z} = -\frac{\omega_{B\alpha}\left(i(\omega\omega_d e_z - V e'_z(\omega_{B\alpha} + V')) + \omega_d e_y(\omega_{B\alpha} + V')\right)}{B_0 D_\alpha \omega} \tag{C5}$$

where $D_\alpha = \omega_D^2 - \omega_{B\alpha}^2 - \omega_{B\alpha}V'$. Equation for e_x separates

$$e''_x = (\omega^2 - k_z^2)e_x, \tag{C6}$$

35

while equation e_y and e_z obey a system of equations

$$e_y = \frac{i}{\omega^2 - k_z^2} \left(4\pi e n_0 \omega (v_{1y} - v_{2y}) + k_z e_z' \right)$$

$$ik_z e_z + e_y' = \frac{4\pi e n_0}{\omega_D} \left(k_z (v_{1z} - v_{2z}) - i(v_{1y}' - v_{2y}') \right) \tag{C7}$$

where velocities can be eliminated using (C5). In full generality the system becomes too complicated to be reproduced here. We consider two simple case: propagation along y-axis and a low frequency limit $\omega \ll \omega_{B\alpha}$.

1. Propagation along z axis

For wave with $e_z = 0$, we can immediately find dispersion relation for the fast mode (inertial Alfvén mode) polarized along y:

$$\omega^2 = k_z^2 + \frac{4\pi n_0 \omega_D^2}{B_0} \left(\frac{\omega_{B1}}{\omega_{B1}^2 + \omega_{B1} V' - \omega_D^2} - \frac{\omega_{B2}}{\omega_{B2}^2 + \omega_{B1} V' - \omega_D^2} \right) \tag{C8}$$

We are interested in low frequency waves $\omega \ll \omega_{B1}, \omega_{B2}$. Assuming that plasma is electron-ion, (first type of particles are electrons with $|\omega_{B1}| \gg \omega_{B2}$), and introducing magnetization parameter

$$\sigma = \frac{\omega_{B2}^2}{\omega_{p2}^2} \tag{C9}$$

we find

$$\omega^2 = k_z^2 + \frac{\omega_D^2}{\sigma} \tag{C10}$$

In the absence of shear this gives dispersion relation for inertial Alfvén waves $\omega = \sqrt{\sigma/(1+\sigma)} k_z c = V_A k_z$ where $V_A = \sqrt{\sigma/1+\sigma} c$ and we have reinstated explicitly the speed of light. This relation is relativistically exact; in the non-relativistic limit $\sigma \ll 1$, this gives so called inertial Alfvén waves with $V_A = \sqrt{\sigma} c = B/\sqrt{4\pi m_p n_0}$.

In the non-relativistic limit $V_A, V \ll 1$ Drift dispersion relation (C10) gives

$$\omega = k_z (V_A \pm V) \tag{C11}$$

2. Oblique propagation normal to the magnetic field : low-frequency limit

Next we consider low frequency waves propagating obliquely to velocity shear. In the limit $\omega \ll \omega_{B2} \ll \omega_{B1}$ we find

$$v_{1y} - v_{2y} = - \left(\frac{\omega_D (k_z \omega_D - (\omega^2 - k_z)^2 V) e_z' - \omega(\omega^2 - k_z^2) e_z V'}{B_0 \omega \omega_{B2} (\omega^2 - k_z^2 + \omega_D^2/\sigma)} \right)$$

$$v_{1z} - v_{2z} = \frac{i\omega_D e_z}{B_0 \omega_{B2}} e_y = \frac{i}{\sigma} \frac{\omega V' e_z + (k_z \sigma + \omega_D)}{\omega^2 - k_z^2 + \omega_D^2/\sigma} \qquad \text{(C12)}$$

which gives an equation for continuous spectrum normal modes

$$\left(\frac{1 + \sigma - V^2}{\sigma(\omega^2 - k_z^2) + \omega_D^2} \right) e_z'' + 2\frac{(\sigma\omega + \omega_D)(k_z - \omega V)V'}{(\sigma(\omega^2 - k_z^2) + \omega_D^2)^2} e_z'$$

$$+ \left(\frac{1 + \sigma}{\sigma} + 2\frac{k_z(k_z - \omega V)V'^2}{(\sigma(\omega^2 - k_z^2) + \omega_D^2)^2} \right) + \frac{(k_z - \omega V)V''}{\omega_D(\sigma(\omega^2 - k_z^2) + \omega_D^2)} \qquad \text{(C13)}$$

Assuming weak non-relativistic shear $V \ll 1$ (neglecting quadratic terms in V), this reduces to

$$\partial_y \left(\frac{1 + \sigma}{\sigma(\omega^2 - k_z^2) + \omega_D^2} e_z' \right) + \left(\frac{1 + \sigma}{\sigma} + \frac{k_z V''}{\omega_D(\sigma(\omega^2 - k_z^2) + \omega_D^2)} \right) e_z'' = 0 \qquad \text{(C14)}$$

This equation is reminiscent of Rayleigh equation in compressible fluid [83]: second derivative of the velocity profile is divided by the shifted drift frequency. This determines the usual Rayleigh instability. (For a flow to be Rayleigh unstable, the necessary condition is presence of inflection point where $V'' = 0$.). [Also note, that for $k_z = 0$ Eq. (C14) gives $\omega = V_A k_y$, so that shear does not affect wave propagation in this case.]

For linear profile $V'' = 0$ and in the non-relativistic limit $V \ll 1$, Eq. (C14) reduces to

$$\partial_y \frac{V_A^2}{\omega_D^2 - k_z^2 V_A^2} e_z' + e_z = 0 \qquad \text{(C15)}$$

Far from the resonance points equation of the form

$$\partial_y \left(f(y) e_z' \right) + e_z = 0$$

with slow varying function $f(y)$ can be solved by WKB method, which gives

$$e_z \propto \frac{1}{\sqrt{f}} \exp\{\pm i \int dy / \sqrt{f(y)}\} \qquad \text{(C16)}$$

Properties of small perturbations on the background flow are closely related to the stability of the flow. Ideal sheared flows may be subject to Kelvin-Helmholtz and Rayleigh instabilities [83]. In addition, in warm plasma new types of instabilities appear, which are related to ion cyclotron motion [34]. Discussion of the stability properties of the transversely sheared flows is beyond the scope of the paper: we assume that the sheared configuration under consideration is stable. This can be shortly justified by noting that Rayleigh-type instability depends on the presence of inflection point in the flow and can be eliminated by choosing, *e.g.* , linear velocity profile, while kinetic instabilities are negligible if the background plasma is cold.
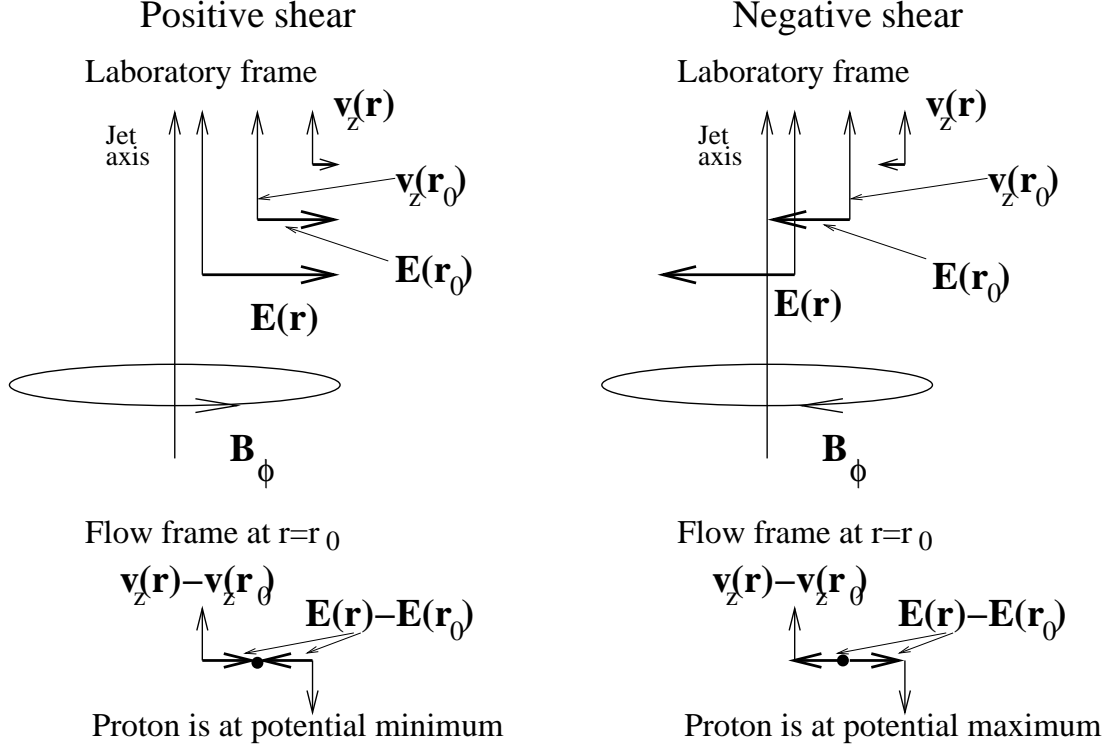
Positive shear

Laboratory frame

Negative shear

Laboratory frame

Flow frame at r=r$_0$

Proton is at potential minimum

Flow frame at r=r$_0$

Proton is at potential maximum

FIG. 1: Potential energy of a charge in a flow for positive and negative shear. Cylindrically collimated flow carries toroidal magnetic field B_ϕ and is sheared, $v_z(r)$, so that regions closer to the axis move with larger velocity. There is an inductive electric field, directed either away from the axis (for positive shear) and towards the axis (negative shear). In a rest frame moving with the flow at some $r = r(r_0)$ the electric field is either towards the origin (for positive shear) or away from the the origin (negative shear), so that a proton is either at potential minimum or maximum.
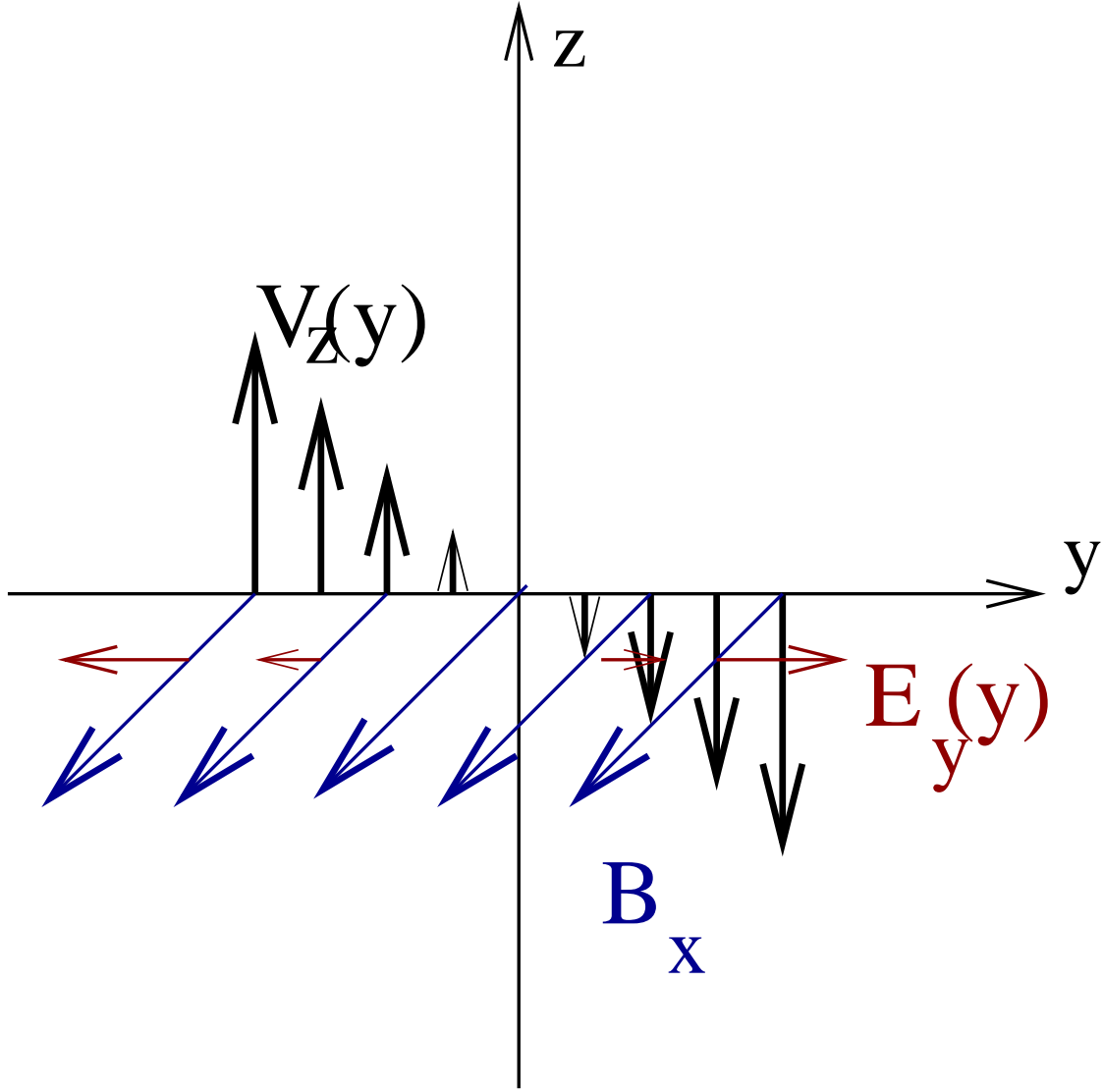
FIG. 2: Electric field in a sheared flow in a frame where surface the $y = 0$ is at rest. For $\mathbf{B} \cdot \nabla \times \mathbf{v} < 0$ the electric field is directed away from the $y = 0$ surface.
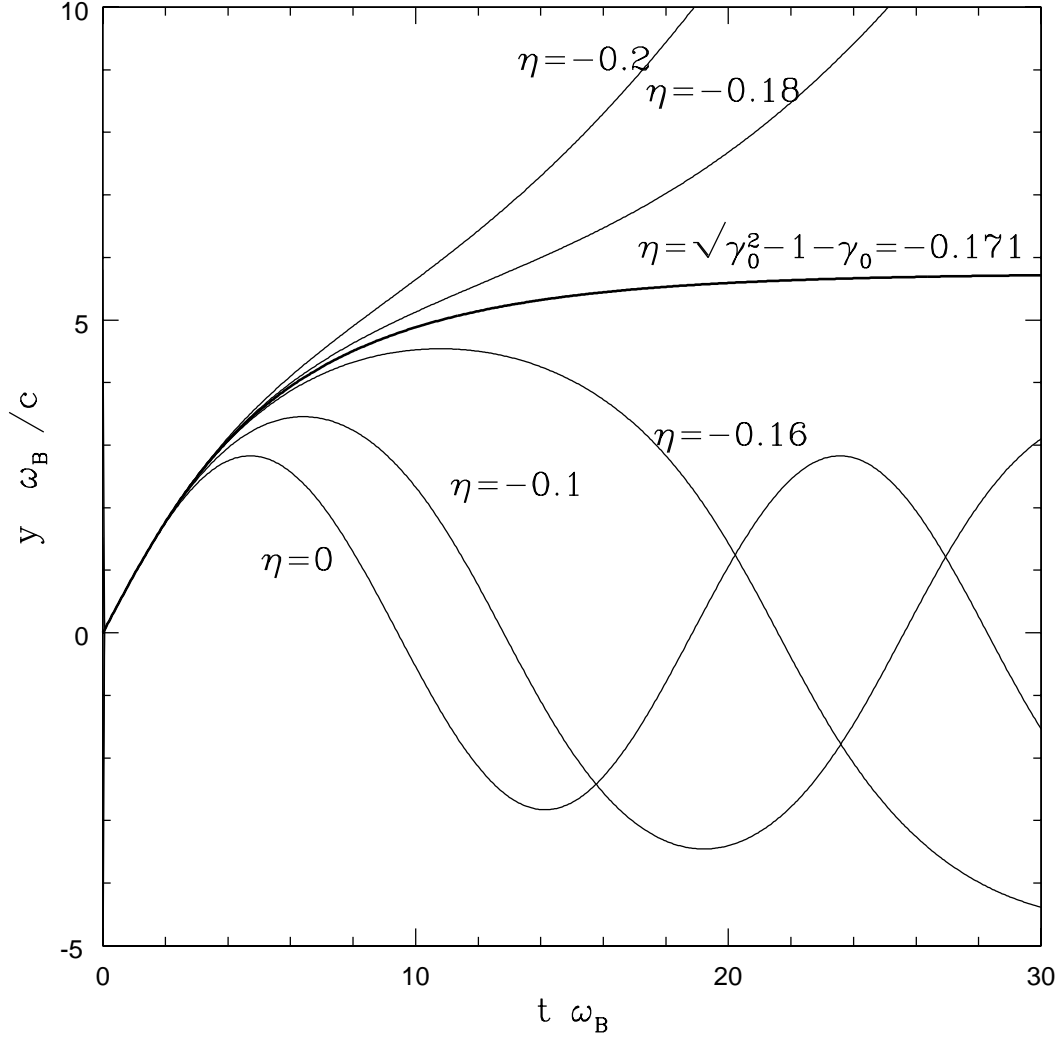
FIG. 3: Particle trajectory $y(t)$ in strongly sheared layers with $v_z(y) = \eta y$ and for different values of η measured in term of the Larmor frequency $\omega_B = eB_0/(mc)$. Magnetic field $B_x = B_0\hat{x}$ is constant. A particle initially at $y = 0$, with velocity along y axes and Lorentz factor $\gamma_0 = 3$. For $\eta < \eta_{crit} = \sqrt{\gamma_0^2 - 1} - \gamma_0 = -0.171$ trajectories are unbound and particle energy increases approximately exponentially, while for larger η trajectories are bound. Particle displacement is measured in term of non-relativistic Larmor radius c/ω_B. For $\eta = \eta_{crit}$ particle reaches $y_{crit} = c/\omega_B\sqrt{1/\eta_{crit}^2 - 1}$ and moves along z axis with constant Lorentz factor $\gamma_{crit} = \gamma_0(1 + \eta_{crit}y_{crit}^2\omega_B/(2c^2))$.
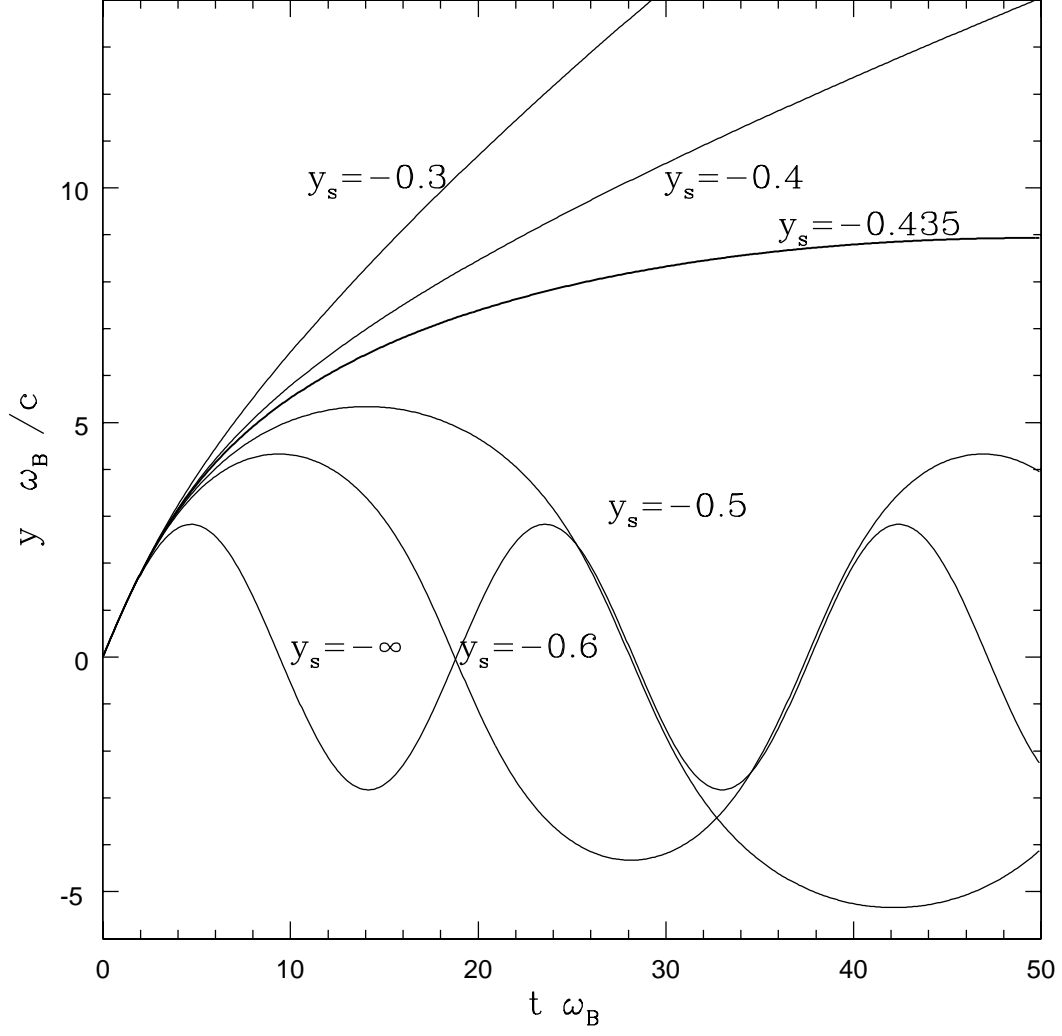
FIG. 4: Same as Fig. 3 but for a velocity profile $V_z = \tanh(y/y_s)$. For $\gamma_0 = 3$, there is a critical values $y_{s,crit} \sim -.435$, so that for $y_{s,crit} < y_s < 0$ particle trajectories are unstable.
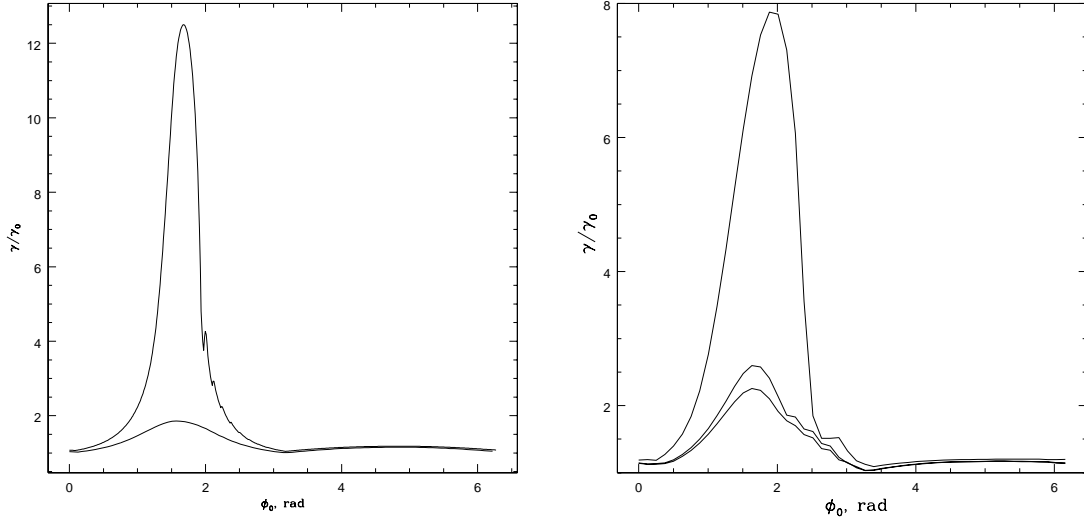
FIG. 5: (a) Maximal energy gained by a particle in a non-linear inertial Alfvén wave propagating in a sheared flow as a function of initial phase of a test particle for the following parameters: $V_A = 0.5c$, $a = 0.25$, $k_z = 0.025$, $y_s = -5$ (both in units c/ω_B), initial energy $\gamma_0 = \sqrt{2}$. Upper curve corresponds to the full case shear plus a wave, lower curve is the case without shear. (b) Dependence of maximal energy gain on shear scale, $y_s = -3$, $y_s = -10$, $y_s = -15$ (top to bottom). In smaller shear (larger negative y_s) acceleration is less efficient.